CENTRO DE INVESTIGACIÓN EN MATERIALES AVANZADOS S.C.

DEPARTAMENTO DE ESTUDIOS DE POSGRADO

Graduate School

Synthesis and characterization of chitosan composites reinforced with carbon nanostructures

(Síntesis y caracterización de compósitos de quitosano reforzados con nanoestructuras de carbono)

THESIS SUBMITTED IN PARTIAL FULLMILMENT OF THE REQUIREMEMENTS FOR THE DEGREE OF

MASTER IN MATERIALS SCIENCE

PRESENTED BY:

Eng. Omar Velázquez Meraz

ADVISOR:

José Martín Herrera Ramírez, Ph.D.

CO-ADVISOR:

Francisco C. Robles Hernández, Ph.D.

CHIHUAHUA, CHIH. **February, 2017**

ABSTRACT

Chitosan is a biopolymer synthesized by the deacetylation of chitin, a natural-occurring polymer found in the exoskeleton of crustaceans. It is known that mechanical properties of biopolymers can be improved by addition of small amount of a reinforcer and an appropriate synthesis technique that allows to homogenously distribute the reinforcer inside the biopolymer matrix.

This work proposes a synthesis based on a thermomechanical process to incorporate carbon nanostructures (CNS) into the chitosan. Chitosan-CNS composites has been synthetized by mechanical milling and conventional sintering. Thermal degradation of chitosan was studied using thermogravimetric analysis (TGA) carried out in an air atmosphere to found optimal sintering temperatures and prevent chitosan degradation. Raw material and prepared composites were characterized using Fourier transform infrared spectroscopy (FTIR), X-Ray diffraction (XRD) and Raman spectroscopy. The morphology and microstructure of the chitosan-CNS composites were characterized by scanning electron microscopy (SEM), bright field transmission electron microcopy (TEM) and optical microscopy (MO). Mechanical properties such as micro and nanohardness as well as elastic modulus were evaluated using Vickers microhardness and nanoindentation tests.

It was demonstrated that the addition of 5 wt% of CNS and sintering at 180 °C for 3 h enhanced the mechanical properties including elastic modulus, micro and nanohardness, which is attributed to the improved cohesion among chitosan and CNS as well as the grain structure refinement due to the mechanical milling.

RESUMEN

El quitosano es un biopolímero sintetizado por la desacetilación de la quitina, un polímero natural que se encuentra en el exoesqueleto de los crustáceos. Se sabe que las propiedades mecánicas de los biopolímeros pueden mejorarse mediante la adición de una pequeña cantidad de reforzante y una técnica de síntesis apropiada que permita distribuir homogéneamente el reforzante dentro de la matriz biopolimérica.

Este trabajo propone una síntesis basada en un proceso termomecánico para incorporar las nanoestructuras de carbono (CNS, por sus siglas en inglés) en la matriz de quitosano. El compósito de quitosano-CNS ha sido sintetizado por molienda mecánica y sinterización convencional.

La degradación térmica del quitosano se estudió mediante análisis termogravimétrico (TGA, por sus siglas en inglés) llevado a cabo en una de aire para encontrar temperaturas óptimas de sinterización y prevenir la degradación del quitosano. La materia prima y los compósitos preparados se caracterizaron mediante espectroscopia infrarroja por transformada de Fourier (FTIR, por sus siglas en inglés), difracción de rayos X (DRX) y espectroscopia Raman. La morfología y microestructura de los compósitos de quitosano- nanoestructuras de carbono se caracterizó con microscopía electrónica de barrido (MEB), microscopía electrónica de transmisión de campo claro (MET) y microscopía óptica (MO). Se evaluaron propiedades mecánicas tales como micro y nanodureza, así como módulo de elasticidad, utilizando microdureza Vickers y ensayos de nanoindentación.

Se demostró que la adición de 5% en peso de CNS y sinterizar a 180 °C durante 3 h incrementan las propiedades mecánicas, incluyendo el módulo de elasticidad, micro y

nanodureza, lo que se atribuye a la mejora de la cohesión entre el quitosano y las CNS así como al refinamiento de la estructura del grano debido a la molienda mecánica.

CONTENT TABLE

FIGURE LIST

TABLE LIST

AKNOWLEDGMENTS

In first place I would like to thank my family for being always there for me and supported me along this path. I also want to thank my friends that, although they may have not supported me directly, they cheered me up in some other ways and from time to time gave me advices that helped me continue. I want to thank all of them for not letting me give up and encourage me to keep on going till the end.

Special thanks to my advisor at CIMAV Dr. Jose Martin Herrera for all his guidance, support and time throughout my Master's program. Special thanks also to my advisor at UH Dr. Francisco C. Robles Hernandez for taking me into his group at UH and for all the help, motivation and guidance during my research stay.

Thanks to my lab mates as well as my class mates at CIMAV for their valuable help and insightful comments. Also thanks the people that help me continue with my work at UH and made of that research stay a valuable lesson.

I would also like to thank all my teachers at CIMAV for all the lessons taught and help whenever I needed it and to all the technicians at CIMAV who helped me during this project.

JUSTIFICATION

In the last years several researches have been carried out in which biomaterials based on polymers are studied that lead to the contribution in the materials science and the bioengineering.

Advances in tissue engineering research on biopolymer structures leading to the construction and regeneration of cells and tissues have made great strides, however this remains a major challenge, because these biopolymeric structures still do not have the ideal mechanical properties to avoid collapsing during treatment or during normal activities of the patient.

Chitosan by itself offers few flexibility in the regulation of mechanical properties and it limits of degradation limit its use. By reinforcing the chitosan through a suitable process that allows them to be distributed and dispersed within the matrix, it will be an effective use to improve its mechanical properties.

CHAPTER 1:

INTRODUCTION

This chapter is intended to perform a literature review to investigate the characteristics and properties of both chitosan and CNS as well as their source and their applications in materials science. In addition, information was consulted about composite materials in general and the characterization techniques that will be used in this work.

1.1 Chitin and chitosan

Chitosan is a polysaccharide obtained by deacetylating chitin, which is the major constituent of the exoskeleton of crustaceous water animals [1].

Chitin is the second most abundant natural polymer, after the cellulose. It is widely found in nature, being invertebrate animals where it is obtained. Insects and crustaceans are probably the best know sources of chitin, with the marine crustaceans the most easily isolated source of chitin available in quantity [2].

Payen [3], in 1943, initiated a controversy that lasted for more than a hundred years on the differences between chitin and cellulose (Figure 1), partly because it was thought that the presence of nitrogen reported in some investigations was due to residues of proteins that could not be completely removed from the samples.

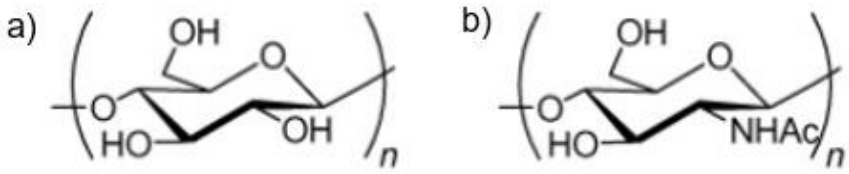

Figure 1. Chemical structure of a) chitin and b) cellulose [3].

Chitin is essentially a homopolymer of 2-acetoamido-2-deoxy-beta-D-glucopyranose. When chitin is further deacetylated to about 50%, it becomes soluble in dilute acids and is referred to as chitosan (Figure 2. Chemical structure of a) chitin, b) chitosan and c) chitosan partially deacetylated [7].). Thus, chitosan is the N-deacetylated derivate of chitin, although the N-deacetylation is almost never complete [4]. There is not a sharp boundary in the nomenclature distinguishing chitin from chitosan. Chitin does occur in nature in the fully acetylated form and has been referred to as chitosan. Chitosan rarely occurs in nature, but is found in the dimorphic fungus, Mucor rouxii. Its occurrence in Mucor rouxii is via the enzymatic deacetylation of chitin [5, 6].

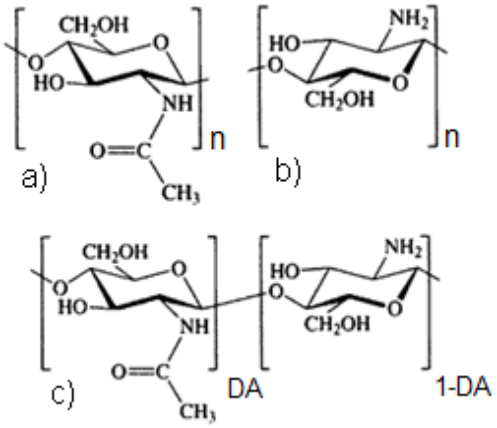

Figure 2. Chemical structure of a) chitin, b) chitosan and c) chitosan partially deacetylated [7].

Chitosan was reportedly discovered by Rouget in 1859 [3], when he boiled chitin in a concentrated potassium hydroxide solution. This resulted in the deacetylation of chitin. Fundamental research on chitosan did not start in earnest until about a century later. In 1934, two patents, one for producing chitosan from chitin and the other for making films and fibers from chitosan, were obtained by Rigby [8].

Chitosan´s primary usefulness is a result of its ability to act as a cationic polyelectrolyte, its bioactivity and biocompatibility, as a thickening agent in water, and selective chelation properties [9]. Chitosan is also readily converted to fibers, films, coatings, and beads as well as powders and solution, which give further enhancing to its usefulness [1].

The chemistry of chitosan is similar to that of cellulose but also reflects the presence of a primary aliphatic amine. Chitosan reacts readily with carbonyl compounds, to form a wide range of ester and amide products [4]. The main driving force in the development of new applications for chitosan lies in the fact that the polysaccharide is not only naturally abundant, but it is also nontoxic and biodegradable [1].

The applications of chitosan are very broad, there are sectors in which its use is usual and known, and others in which it is currently an interesting research route [10]. When chitosan is reinforced, its properties improve and therefore its applications (Table 1) go beyond its usual applications, so that the development of multi-functional bio-composites is a topic of great interest in the fields of material science and bioengineering [11].

Table 1. Some examples of chitosan reinforced applications [11].

Application	**Suitability/ Properties**
Artificial skin	Renewable, nontoxic, bioactive
Sutures	Biocompatible, biodegradable
Wound dressing	Antibacterial, antiviral, antifungal, nontoxic
Implants	Biocompatible, biodegradable
Bone reconstruction	Biocompatible, nontoxic, bioactive, film-forming
Corneal contacts lenses	Hydrating ability
Controlled drug release	Biocompatible, nontoxic, water permeable

1.2 Carbon nanostructures

Carbon nanostructures (CNS) are defined as those carbon materials that are produced on a scale of nanometer size (less than 100 nm). The existence of the wide variety of structures and nanostructures of carbon are due to the ability of the carbon to hybridize its electronic configuration to sp2 and sp3 with almost identical energies [12].

These CNS have been considered as reinforcing materials ideal for polymer matrices to achieve high performance and give them a multifunctional character due to their nanometric size, high aspect ratio and, above all, their extraordinary mechanical strength [13].

1.2.1 Fullerene soot

Fullerene soot is a fine powder composed of a mix of C_{60} and C_{70} fullerenes in a ration of roughly 22% C_{60} and 76% C_{70}. This CNS are a notable material for its versatility in the synthesis of new compounds and also is an effective reinforcer for structural applications [12].

The fullerene field was revolutionized by the discovery that simple vaporization of graphite rods could produce fullerenes in substantial yield. This procedure, which is often termed the Krätschmer-Huffman method, is a straightforward and low cost method for generating large quantities of fullerene. The Krätschmer-Huffman arc-discharge consists of evaporating graphite electrodes via restrictive heating in a helium atmosphere. The resulting soot contains a few percent of fullerenes which could be extracted with benzene as solvent. This was the first method to produce gram-sized samples [14].

The method was later on modified by Smalley who established an electric arc between two graphite electrodes, where most of the power dissipates in the arc [14].

1.3 Composite materials

Composite materials are multiphase materials obtained through the combination of different materials in order to attain properties that the individual components by themselves cannot attain [15]. They are not multiphase materials in which the different phases are formed naturally by reactions, phase transformations, or other phenomena. Composite materials can be tailored for various properties by appropriately choosing their components, proportions, distributions, morphologies, degrees of crystallinity, crystallographic textures, as well as the structure and composition of the interface between components [16].

1.3.1 Composite materials structure

The structure of a composite is commonly such that one of the components is the matrix while the other component is filler bound by the matrix, which is often called binder [17].

Composites can be classified according to the matrix material, which can be a polymer, a metal or a ceramic. They can also be classified according to the shape of the filler. A composite that has particles as the filler is said to be a particle composite. A composite with fibers used as the filler is said to be a fibrous composite. The components in a composite can also take the form of layer [16, 17].

1.3.2 Properties of composite materials

The properties of a composite are a function of the properties of constituent phases and their relative proportions, size, shape, distribution, and orientation of the dispersed phase.

The proportion of constituents can be expressed either by weight fraction or by volume fraction. The weight fraction is relevant to fabrication and the volume fraction is commonly used in property calculations [15, 16].

A good distribution and dispersion of the reinforcer is usually an essential requirement to give a high yield to the composite (Figure 3). The distribution describes the location of the reinforcer within the matrix, while the dispersion refers to the breakage of aggregates in small sizes [18].

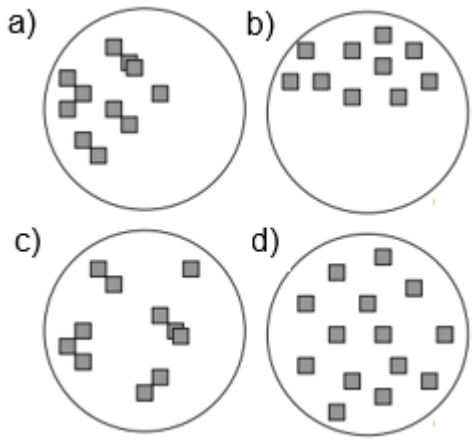

Figure 3. Possible distribution and dispersion of the reinforcer in the matrix: a) Bad distribution and bad dispersion, b) Bad distribution but good dispersion, c) Good distribution but bad dispersion and d) Good distribution and good dispersion [18].

1.4 Biopolymer composites

Novel biomaterials in the form of composites with nanosized reinforcers may bring unpredictable new characteristics to a material, such as mechanical, physical, optical, chemical reactivity, electric and magnetic properties, in addition to new functionalities that may be unavailable at macroscale [11].

During recent years, an extensive interest has arisen in the development of product from bio-based and natural resources, and their extensive use in a variety of applications including biomedical products for wound dressing, artificial skin, structures, and the controlled release

of drugs. It is well known that naturally occurring polymers have a greater biocompatibility and immunogenicity than synthetic polymers when used in biomedical applications [10, 11].

Conventional polymer-processing methods such as melt extrusion, compression molding or injection molding have not been reported for biopolymer-based composites intended for medical application [19].

In biopolymer composites, filler dispersion and interfacial interactions are the crucial parameters for improving mechanical properties, low dispersion and interfacial bonding limit the full use of CNS to reinforce the polymers, making it necessary to optimize the transformation conditions. To achieve good dispersion and good interactions with the polymer chains, a solution could be done by introducing a coupling agent capable of reacting with the two phases [18].

Polysaccharide-based polymers such as cellulose, chitin, and chitosan represent another class of polymers used to develop biomaterials for medical applications [19].

Chitosan composites have potential biomedical applications, owing to its good biocompatibility, and its nontoxic, biodegradable, and inherent wound-healing [20].These composites has a potential use in skin repair and regeneration subsequent to injuries or burns compared to the use of pure chitosan which is a rigid and brittle material and offers a low elasticity for the desired application [21].

1.5 Mechanical milling

Mechanical milling is a process that is performed in high energy ball mills where the powder that is deposited in their interior is welded, broke and re-welded. The aim is to reduce the particle size, change its shape or create mixing processes and welding, obtaining a fine and controlled microstructure of metallic powders, polymers, compounds and ceramics [22].

Particle size reduction, or comminution is an important step in many technological operations. The process itself is defined as the mechanical breakdown of solids into smaller particles without changing their state of aggregation. It may be used to create particles of a certain size and shape (including nanosize), to increase the surface area and induce defects in solids which is needed for subsequent operations such as chemical reactions, sorption, etc. Milling not only increases the surface area of solids. It is likely to increase the proportion of regions of high activity in the surface [23].

1.6 Sintering

Sintering may be considered the process by which an assembly of particles, compacted under pressure or simply confined in a container, chemically bond themselves into a coherent body under the influence of an elevated temperature. The temperature is usually below the melting point of mayor constituent [24].

The nature and strength of the bond between the particles and, consequently, the sintered compacted, depend on the mechanisms of diffusion, plastic flow, recrystallization, grain growth and pore contraction. Also, according to the temperature and time of sintering, different structures and porosities can be obtained in a sintered tablet, allowing to modify its properties [25].

1.7 State of the art

In order to know what has been studied at the moment on the subject of the reinforced chitosan, the most recent research papers were consulted, among which the most relevant are mentioned below:

In 2005, the work "Preparation and Mechanical Properties of Chitosan / Carbon Nanotubes Composites", in which the authors S.F. Wang, L. Shen, W.D. Zhang and Y.J. Tong propose a solution-evaporation synthesis to synthesize chitosan composites with carbon nanotubes [26].

In 2012 the authors A. Aryaei, A.H. Jayatissa, A.C. Jayasuriya and J. Mech. Behav are able to synthesize chitosan-calcium-phosphate composites by the uncrossed-linked method, where the chitosan is cross-linked with triphosphate (TPP) and then mixed with the calcium phosphate matrix [27].

In 2016, Nawrotec and his collaborators proposed a synthesis by tubular electrodeposition of chitosan with carbon nanotube to produce composites enriched with calcium ions [28].

In the same year, the authors M. Fardioui, M. Mekhzoum, A. Kacem and R. Bouhfid synthetized bionanocomposite materials based on chitosan reinforced with cellulose and organo-modified montmorillonite [29] .

In this work it is proposed to synthesize the composites by means of a thermomechanical process that involves the mechanical milling, which is a technique that produces highly homogeneous nanostructured materials, improves integrity and has positive effects on mechanical properties; and by conventional sintering, which is a process where chitosan and CNS powders are consolidated and whose nature is preserved while improving upon the material properties.

HYPOTHESIS AND OBJECTIVES

Hypothesis

It is possible to produce chitosan composites with CNS through a thermomechanical process involving mechanical milling and sintering techniques in order to improve the mechanical properties (elastic modulus and micro and nanohardness) of chitosan.

General objective

To establish the optimum conditions for sintering and processing of composites chitosan-CNS using mechanical milling and conventional sintering, in order to increase the mechanical properties of the composites.

Specific objectives

• To evaluate the main properties of the raw material in order to guarantee its purity.

• To synthesize the composites by the mechanical milling process, as well as to evaluate the morphology of the ground product obtained by this technique.

• To experiment with different compositions of CNS, sintering temperature and sintering time, in order to select the ones that provide the best mechanical properties.

CHAPTER 2

EXPERIMENTAL METHODOLOGY

This chapter is conceived to know the different experimental techniques, procedures and equipment used in this work, as well as the preparation techniques and the conditions under which they were developed.

2.1 Mechanical milling

Samples were prepared using low molecular weight chitosan powder (Sigma-Aldrich®, St. Louis, MO) with a deacetylation degree of 80% and commercially available fullerene soot (SES Research, Houston, TX) as CNS.

Mechanicall milling was performed in an High Energy SPEX 8000 mixer/mill (Figure 4) using a stainless steel vial as a container for the sample and with a ball-to-powder weight ratio of 10:1.

Chitosan was milled for 5, 10, 15, 20 and 25 h and CNS for 3 h. Finally, the chitosan-CNS composite samples were mixed at a 99:1, 97:3 and 95:5 weight ratio (chitosan-CNS) and milled together for an additional hour.

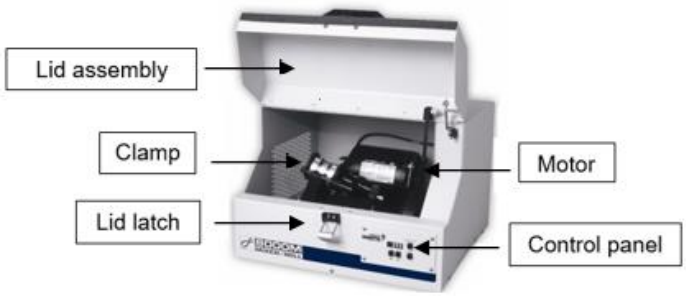

Figure 4. SPEX 8000 mixer/mill and its main components.

2.2 Sintering

Sintering process was performed on a custom made French press-heater (Figure 5). The temperature was monitored via a high speed, high resolution data acquisition system (NIcDAQ-9174: National Instruments, Austin, TX) coupled to the equipment and measured with a K-type thermocouple.

The sintering was conducted at 120, 150, 180 and 220 ºC for 3 and 5 h .These sintering temperatures were obtained based in the criteria that sintering temperature (Ts) should be conducted at Ts= (0.7-0.8) Tm [30], where Tm represent the melting point, in this case degradation and decomposition temperature. All experiments were carried out in an air atmosphere and under a constant pressure of 3.5 MPa through the entire sintering process.

The temperature during sintering was measured in close proximity to the die (Figure 5). Through calibration of the equipment, it was determined that the sintering temperature can be up to 30° C lower to that measured by the thermocouple. This temperature was used to offset the collected data.

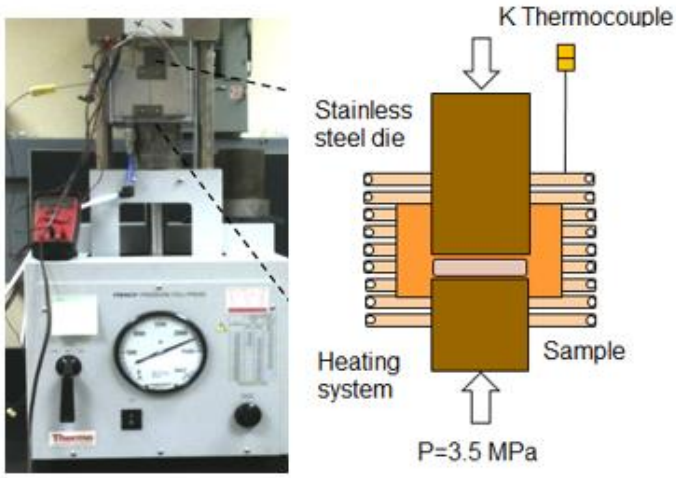

Figure 5. French press and custom designed heater system.

2.3 Experimental design

Once the mechanical milling and sintering conditions were set up, the chitosan-CNS composites were synthesized. A nomenclature was used to identify the samples (Table 2 and Table 3), where the first term represents the sintering time; the second term represents the reinforcer (CNS) content in the chitosan matrix expressed in weight percent (wt%), finally, the last term represents the sintering temperature.

As can be observed, for each temperature and sintering time condition there exists a sample of sintered chitosan without reinforcer, these samples are denominated "control samples", and they are used to make a comparative analysis of diverse characterization techniques with the chitosan-CNS composites and their respective sintering conditions.

Table 2. Samples of chitosan sintered for 3 h.

3 h 0% 120 °C	3 h 0% 150 °C	3 h 0% 180 °C	3 h 0% 220 °C
3 h 1% 120 °C	3 h 1% 150 °C	3 h 1% 180 °C	3 h 1% 220 °C
3 h 3% 120 °C	3 h 3% 150 °C	3 h 3% 180 °C	3 h 3% 220 °C
3 h 5% 120 °C	3 h 5% 150 °C	3 h 5% 180 °C	3 h 5% 220 °C

Table 3. Samples of chitosan sintered for 5 h.

5 h 0% 120 °C	5 h 0% 150 °C	5 h 0% 180 °C	5 h 0% 220 °C
5 h 1% 120 °C	5 h 1% 150 °C	5 h 1% 180 °C	5 h 1% 220 °C
5 h 3% 120 °C	5 h 3% 150 °C	5 h 3% 180 °C	5 h 3% 220 °C
5 h 5% 120 °C	5 h 5% 150 °C	5 h 5% 180 °C	5 h 5% 220 °C

2.4 Physico-chemical properties

The physicochemical properties of chitosan affect its functionality and also vary depending on the source and method of obtaining the chitin, the method and the deacetylation conditions, as well as the methods and conditions for the determination of the physico-chemical properties [31].

It is important to evaluate these physicochemical properties for any use that will be given to chitosan, as this will allow to know the functionality of the material regardless of its origin.

The physicochemical properties of chitosan that mainly influence the functionality of chitosan are: viscosity, molecular weight and degree of deacetylation, all closely related.

2.4.1 Determination of the deacetylation degree

The degree of deacetylation is defined as the amino group content present in the polymer chain and is expressed by the percentage of free amino groups in the chitosan molecule and is closely related to its solubility [32].

The determination of the content of amino groups in the chitosan is carried out by an acid-base potentiometric titration, a method proposed by Broussignac [33], which consists in measuring the variations of the pH values to the titrator in a chitosan solution.

For the potentiometric titration, 0.5 g of chitosan was dissolved with an excess of hydrochloric acid (HCl) 0.2 M to protonate the free amino group of the chitosan and then carry out a titration with sodium hydroxide (NaOH) 0.1 M until the pH of the solution is stabilized. Every 2 ml of NaOH added to the solution pH was measured with a pH potentiometer.

With the data obtained a potentiometric curve was constructed. Then a curve of titration with two inflection points is generated, whose values were determined according to the criterion of the first derivative. This difference between these points gives the ratio of the amount of acid required to protonate the amino groups of chitosan. The calculation of the concentration of the amino groups (% NH_2) can be determined by the following equation [33].

$$\% NH_2 = \frac{16.1\,(y-x)}{w}\, f \qquad (1)$$

Where y is the mayor inflection point and x the lowest (both expressed as volume)

f is the molarity of the NaOH solution

w is the mass of the simple in grams

16.1 is a factor associated with the type of protein under study

2.4.2 Molecular weight

Chitosan is a polymer made up of repeating units of D-glucosamine, so the chain length and, therefore, its molecular weight, is an important feature of the molecule. The molecular weight affects the physical and chemical properties of chitosan, as well as its functionality. Therefore the determination of the molecular weight is very important to elucidate the characteristics of the own chitosan as of its products [31].

Knowing the intrinsic viscosity the molecular weight of the sample analyzed can be analyzed, as long as the polymer obeys the Huggins equation [34] (equation 2); that is, if it presents a linear behavior between the concentration and the reduced viscosity:

$$\frac{n_{sp}}{C} = [n] + K[n]^2 C \qquad (2)$$

The intrinsic viscosity measures the effective specific volume of an isolated polymer, reason why its determination is extrapolating to zero concentration (equation 7).

The value of the intrinsic viscosity depends on the size and shape of the solute molecule, as well as its interaction with the solvent and the working temperature. For the polymer-solvent system, the Mark-Houwink equation (equation 3) [35] can be used to determine the average molecular weight of the polymer.

$$\mathrm{Mv} = ([\mathrm{n}]/1.181\mathrm{x}10^{-3})^{1/0.93} \quad (3)$$

To determine the molecular weight of the chitosan, a Brookfield viscometer (Figure 6) equipped with a cooling bath was used. For the analysis 10 ml volumes of solution of chitosan at room temperature, using a number 18 spindle and a turning speed of 1000 RPM, were used. The solution of chitosan was prepared by dissolution in a mixture of acetic acid 0.1 M and sodium chloride 0.2 M. Several concentrations of chitosan were used for the analysis ($2.0\mathrm{x}10^{-3}$, $4.0\mathrm{x}10^{-3}$, $6.0\mathrm{x}10^{-3}$ and $8.0\mathrm{x}10^{-3}$ g/ml).

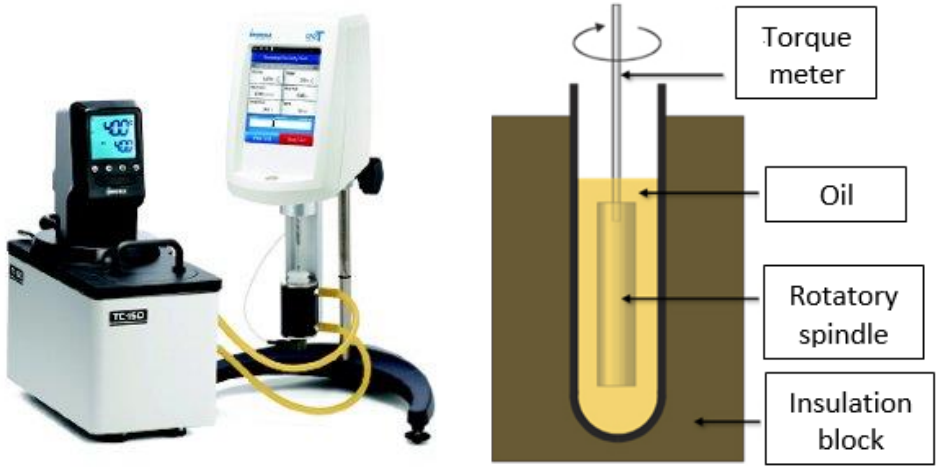

Figure 6. Brookfield viscometer DV 2T and its main components.

With the data obtained, equations 4-6 [31] were used to obtain the reduced viscosity from the viscosity measured, then the points corresponding to the reduced viscosities were plotted with respect to the concentration, and a linear regression of these were taken from the above equations; the intrinsic viscosity and then the molecular weight were determined.

$$n_r = \frac{n}{n_o} \tag{4}$$

Where: η is the viscosity of the solution

η_o is the viscosity of the pure solvent

Specific viscosity: $\mathrm{n_{sp}} = \mathrm{n_r} - 1$ (5)

Reduced viscosity: $\mathrm{n_{red}} = \left(\frac{\mathrm{n_{sp}}}{\mathrm{C}}\right)$ (6)

Intrinsic viscosity: $[\mathrm{n}] = \left(\frac{\mathrm{n_{sp}}}{\mathrm{C}}\right)_{\mathrm{C}\to\infty}$ (7)

2.5 CHNS elemental analysis

Carbon, hydrogen, sulphur and nitrogen contents of chitosan were determinated using CE instruments EA 110 CHNS-O Elemental Analyzer (Figure 7) .

Figure 7. CE EA 1110 CHNS Elemental Analyzer.

For this analysis, a small amount of chitosan was weighed in tin capsules and then introduced into a vertical quartz reactor heated at a temperature of 1020 °C with a constant flow of helium stream. A few seconds before introducing the helium stream was enriched with high purity oxygen.

The combustion gas mixture produced by the chitosan sample was driven through a tungsten oxide zone to achieve a complete quantitative oxidation followed by a reduction step in a copper zone to reduce nitrogen oxides and sulfuric anhydride to nitrogen and sulfurous anhydride.

The resulting four components N_2, CO_2, H_2O and SO_2 were separated in a chromatographic column and detected by a thermos conductivity detector.

The resulting signals, proportional to the amount of eluted gases, were analyzed by an automatic workstation, which provided the sample elemental composition report.

Analysis was performed in a tin boat sample pan at a combustion temperature of 1150 °C and at a reduction temperature of 850 °C. Gas flow rate was 200 ml/min and 14 ml/min for helium and oxygen respectively, a whole diagram of the equipment can be seen in Figure 8.

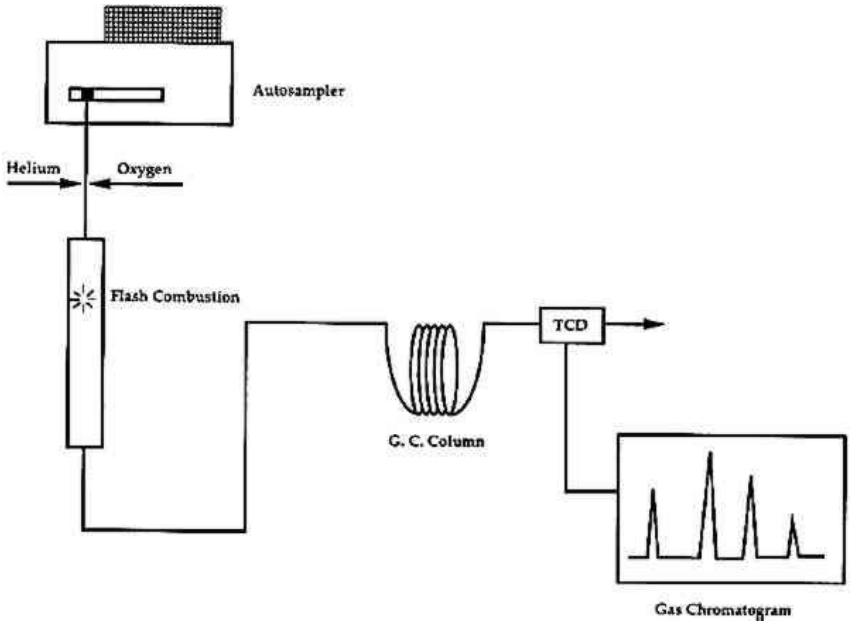

Figure 8. Diagram of an elemental analyzer [36].

2.6 Thermal analysis

TGA was used to evaluate the thermal stability of chitosan and CNS, as well as to determine the degradation temperature of chitosan with both TGA and DSC curves. Thermogravimetric measurements were made using a DSC Auto sampler developed by TA instrument (Figure 9) with a microprocessor driven temperature control unit and a TA data station. The mass used of the samples for every sample was generally in the range of 2-3 mg.

The sample pan was placed in the balance system equipment and the temperature was raised from 25 to 700 °C at a heating rate of 5 °C/min under an air atmosphere. In the case of CNS, temperature was raised from 25 to 900 °C at a heating rate of 10 °C/min under an air atmosphere. The mass of the sample pans were continuously recorded as a function of temperature.

Figure 9. DSC Auto sampler, TA instruments.

2.7 Infrared spectroscopy

Chitosan and chitosan-CNS composites were characterized by infrared spectroscopy in the region comprising from 500 to 4000 cm^{-1}. Absorption spectra were obtained on a Fourier transform spectrophotometer Perkin Elmer (Figure 10).

The powdery chitosan was mixed thoroughly with KBr and then pressed to a homogeneous disc with a thickness of 0.5 mm. The discs were scanned in the region previously mentioned to obtain FTIR spectra.

No preparation of chitosan-CNS composites was done because they were already in bulk form.

Figure 10. FTIR Spectrometer Perkin Elmer.

An important data that can be obtained across the chitosan spectrum is the actual value of the degree of deacetylation by means of the Bruggnerotto equation (equation 8) [37] and the correlation of some vibration bands associated with the acetyl group. Appling equation 9, degree of deacetylation of chitosan was determined.

$$Nac(\%) = 31.92 * \frac{A1318}{A1380} - 12.2 \quad (8)$$

$$DA(\%) = 100 - Nac(\%) \quad (9)$$

2.8 Raman spectroscopy

For the development of this work, a confocal micro-Raman XploRA, Horiba JY (Figure 11) was used; this device is equipped with 3 lasers: 532 nm, 638 nm and 785 nm, as well as 2 optic lenses: 10x and 100x. High numerical aperture microscope objectives greatly enhance the spatial resolution and the optical collection power of the Raman instrument [30].

Figure 11.Raman Spectrometer HORIBA XploRA.

For all samples, a 638 nm diode was used to analyze the samples along with a 10x optic lens for the chitosan and 100x for the chitosan-CNS composites and CNS powders. The details of the equipment specifications are presented in Table 4.

Table 4. Raman's instrument specifications.

Spectral range	20 cm^{-1} to 1200 cm^{-1}
Spectrograph:	Imaging flat field spectrometer
Detector:	CCD detector
Microscope	Materials/clinical light microscope, Horiba
Confocal sampling	Rugged confocal spatial filtering

2.9 X-ray diffraction

The technique of X-ray diffraction was used to analyses all samples. X-ray diffractograms of chitosan-CNS composites, samples of chitosan at different milling time and CNS with and without milling were obtained in order to observe the milling effect in each one of them, find

their phases and calculate the crystallinity index; this last for chitosan samples and chitosan-CNS composites.

The crystallinity index is determined by the method of signal intensity proposed by Focher and his collaborators [38].

The crystallinity index is calculated according to the following equations:

$$CI\% = [(I_{110} - I_{am})/I_{110}] * 100 \quad (10)$$

$$CI\% = [(I_{020} - I_{am})/I_{110}] * 100 \quad (11)$$

Where I_{110} (arbitrary units) is the maximum intensity of the (110) peak, I_{020} (arbitrary units) the maximum intensity of the (020) peak and Iam is the amorphous diffraction at 2θ = 12.6° (arbitrary units) [38].

For this analysis, a D8 Advance X-ray diffractometer developed by Bruker (Figure 12) was used under different conditions, which are displayed in Table 5.

Figure 12. Bruker D8 Advance diffractometer.

No preparation of samples was done because chitosan and CNS were already in powder form and the chitosan-CNS composites in bulk form.

Table 5. X-ray diffractometer conditions.

Sample	Step (Deg.)	2θ range (Deg.)	Step time (s)	Cu K_α radiation (Å)
Chitosan	0.05	5-50	70	1.5418
CNS	0.01	10-50	70	1.5418
Chitosan-CNS composites	0.05	5-50	70	1.5418

2.10 Density

Densities of the chitosan-CNS composites were obtained with a Sartorius YDK01 Density Determination Kit coupled to an analytic balance (Figure 13). Here, the relationships between the mass, the volume and the density of solid bodies immersed in liquid, as described by Archimedes form a basis for the determination of the density of substances.

Archimedes principle establishes that a solid immersed in a liquid is subjected to the force of buoyancy. The value of this force is the same as that of the weight of the liquid displaced by the volume of the solid [39].

Figure 13. Sartorius balance with a YDK01 density determination kit.

Then, according to the previously mentioned, the beaker was placed on the pan of the balance and the sample-holding device was immersed in the liquid (in this case ethanol was used), to the same depth that the samples were immersed on it. The weighing instrument is tared. The samples was placed next to the beaker on the weighing pan. The weight of the sample in air w_a (g) was determined. The samples were placed in the holding device on the stand and immersed in the liquid. The weight readout shows the displaced liquid w_f (g).

For every analysis temperature of the ethanol was read off to find the density ρ (fl) of the liquid (in g/cm^3). Finally, the buoyancy (G) is calculated by the equation 12 [17] and the specific gravity was calculated using the equation 13. Air buoyancy is considered in equation 13 [39], as well as the additional buoyancy, caused by the immersed part of the measuring device by the geometry of the measuring device setup used in this analysis.

$$\mathrm{G} = \mathrm{w_a} - \mathrm{w_f} \tag{12}$$

$$\rho = \frac{w_a[\rho(fl) - 0.0012 g/cm^3]}{0.99983\ G} + 0.0012\ g/cm^3 \tag{13}$$

2.11 Porosity

The porosity of the samples was determined to observe the effect of pore contraction by sintering. For this purpose, samples were cut into small pieces and dimensioned in order to obtain pieces with a uniform volume (Vc) without considering the volume of the pores. The pieces were weighed on an analytical balance to obtain the weight of the dried pieces (w1) and placed in a 10 ml beaker to be topped with ethanol of known density; then they were placed in a freezer for 40 minutes. After that the pieces were removed and the weight of the wet pieces (w2) was taken, in order to calculate the volumes of the pores (Vp) by means of the equation 15 [40]; obtaining this volume the equation 16 [40] was used to obtain the

volume of the skeleton of the pieces. Finally, with the data obtained, the percentage of porosity of the pieces was calculated by means of the equation 17 [40].

$$\rho\ \text{ethanol} = \frac{\text{w ethanol}}{\text{V ethanol}} \tag{14}$$

$$\text{Vp} = \frac{\text{w2}-\text{w1}}{\rho\ \text{ethanol}} \tag{15}$$

$$\text{Vc} = \text{Vs} + \text{Vp} \tag{16}$$

$$\%\ \text{porosity} = \left(\frac{\text{Vc}-\text{Vs}}{\text{Vc}}\right) * 100 \tag{17}$$

2.12 Scanning electron microscopy

The interaction of the electron beam with the sample produces different signals, as shown in Figure 14. In this work, secondary electrons and back-scattered electron were used to analyze the samples.

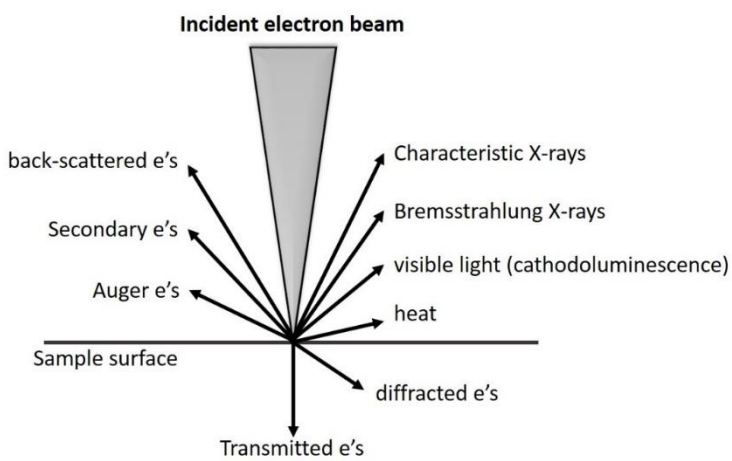

Figure 14. Types of interactions between electrons and sample [41].

The morphologies of chitosan samples and chitosan-CNS composites were observed in a HITACHI SU3500 (Figure 15a), operated under 15 kV in low vacuum mode (50 MPa) and a signal of back-scattered electrons.

The CNS were examined in a field emission JEOL JSM-7401F (Figure 15b), operated under 5 kV with a signal of secondary electrons in order to get high resolution micrographs.

Figure 15. Scanning electron microscopes. (a) HITACHI SU3500, (b) JEOL JSM-7401F.

2.13 Transmission electron microscopy

The CNS and chitosan-CNS composite morphology were observed in a transmission electron microscope HITACHI HT7700 (Figure 16) using transmitted electrons signal (bright field).

Figure 16. Transmission Electron Microscope HITACHI HT7700.

CNS samples were prepared by the powder dispersion method, in which a solution was prepared by dispersing the CNS particles by means of ultrasound. Subsequently, a small amount of sample was taken with a capillary and deposited on a copper grid; then was allowed to dry the solvent.

In the case of the chitosan-CNS composite only a small sample was taken from the specimen to be investigated, so an extremely thin sections was obtained from the bulk material with a Power Tome Ultramicrotome (Figure 17) equipped with a glass knife.

Here, a representative composite sample was cut with a diamond wafer blade in order to get a small piece similar to a pyramidal form and it was cold-mounted with epoxy resin. Once the piece was mounted, machinery was necessary to dimension the sample and place it in the ultramicrotome to get a small thin section. Finally, this thin section was deposited in a copper grid.

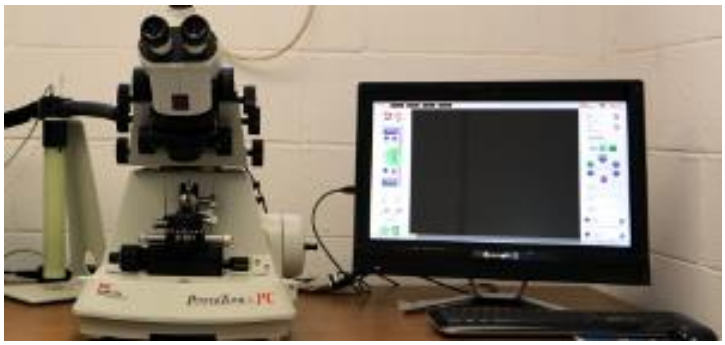

Figure 17. PT-PC Power Tome ultramicrotome.

2.14 Vickers microhardness

For chitosan-CNS composites microhardness analysis, the Vickers method was used on a Microdurometer LM 300 AT (Figure 18) with a load of 200 g_f and dwell time of 10 s.

In order to examine the chitosan-CNS composites, small pieces were cut from the composites with a diamond wafer blade and they were cold-mounted in epoxy resin. The mounted pieces were grinded with coated abrasive papers of SiC and then polished.

For each sample, 6 measurements were performed in a different zone and the results were averaged.

Figure 18. Microdurometer LECO Series LM 300 AT.

2.15 Nanoindentation

Nanoindentation tests were performed to determine the mechanical properties at the local level of the different chitosan-CNS composites. Mechanical properties such as hardness (H) and elastic modulus (E) were evaluated in a Nano Indenter G200 (Figure 19) coupled with a DCM II head.

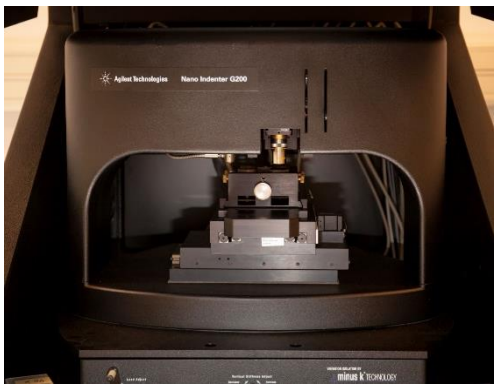

Figure 19. Nano Indenter G200.

For this analysis, a Berkovich indenter tip was used. This tip is the most frequently used indenter tip for instrumented indentation testing to measure mechanical properties at the nanoscale. Specifications of the Berkovich tip used in this work is shown in Table 6.

Table 6. Berkovich tip specifications.

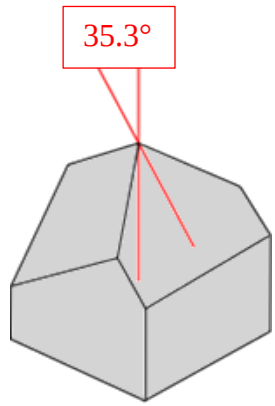

Figure 20. Nanoindenter Berkovich tip.

For the sample preparation, small pieces were cut from the composites with a diamond wafer blade and directly grinded with coated abrasive papers of SiC and then polished (no resin-mounting was used for this analysis).

Nanoindentation tests were performed in a system with real-time data collection. The applied load was 0.2 mN and reported values are the average of 4 measurements.

Table 6. Berkovich tip specifications.

Tip	Berkovich
Shape	3-sized pyramid
Centerline-to-face angle (α)	35.2644°
Area (projected), A(d)	2.5981d2
Volume-depth relation, V(d)	0.8657d3
Projected area/face area (A/Af)	0.5774
Equivalent cone angle (ψ)	42.28°

2.16 Optical microscopy

An optical Axio Scope A1 polarized light microscope developed by Zeiss, equipped with ICc5 camera and AxioVision Rel. 4.8 Software for Image Acquisition and Management, was used in bright field mode (Figure 21).

Chitosan-CNS composites sample previously polished (see section 2.6) were cleaned with ethanol and were examined under the optical microscope at high magnifications.

Figure 21. Axio Scope A1 microscope.

CHAPTER 3

RESULTS AND DISCUSSION

In this chapter the characterization results of the chitosan, CNS and chitosan-CNS composites will be presented and discussed.

3.1 Elemental analysis

Table 7 presents the elemental composition of chitosan. Comparing with the literature [42] the composition obtained through this technique fulfills the one of the theoretical elemental composition.

Table 7. CHNS elemental analysis for chitosan.

Sample	C %	H %	N %	S %
Theoretical	40.68	6.21	7.90	0
Chitosan	41.30	7.22	7.55	Not detected

3.2 Determination of the deacetylation degree

The results of the titration are shown in Figure 22a, through this information a curve is produced with two inflection points as shown in Figure 22b, whose values were determined according to the criterion of the first derivative.

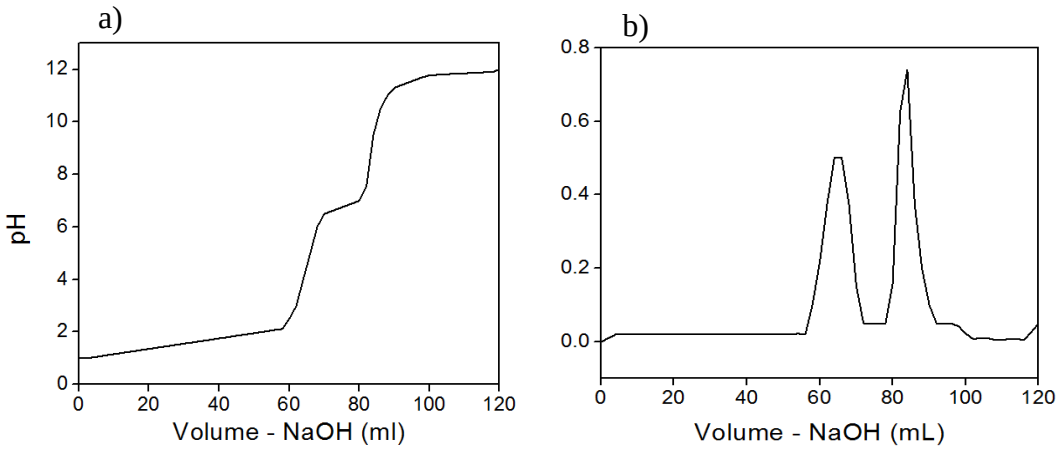

Figure 22. a) Titration curve of chitosan and b) criterion of the first derivative.

By means of equation 1 and the parameters shown in Table 8 for the potentiometric titration, a degree of deacetylation of 64.4% was obtained. It is important to note that chitosan is defined as chitin which has been deacetylated at 60-75% or more, at which point it becomes soluble in organic acids [43].

Table 8. Parameters obtained in the potentiometric titration.

w (g)	y (ml)	x (ml)	f (mol/L)	NH_2 (%)
0.5	82	62	0.1	64.4

3.3 Determination of the molecular weight

Table 9 shows the results of the measured viscosity of chitosan solutions at different concentration. Reduced viscosity was calculated applying equations 4-6 and was adjusted to the Huggins equation (equation 2).

Table 9. Parameters of the viscosity tests of the chitosan sample.

Amount of Chitosan used (g)	Concentration (g/ml)	Viscosity of the solvent(cP)	Viscosity (cP)	Reduced viscosity (ml/g)
1.00	0.002	12.10	20.70	397.15
2.00	0.004	12.10	43.73	653.52
3.00	0.006	12.10	80.89	947.65
4.00	0.008	12.10	135.33	1273.04

Figure 23 shows the linear regression of the reduced viscosity points as a function of the concentration for the sample of chitosan evaluated, where a linear behavior is observed.

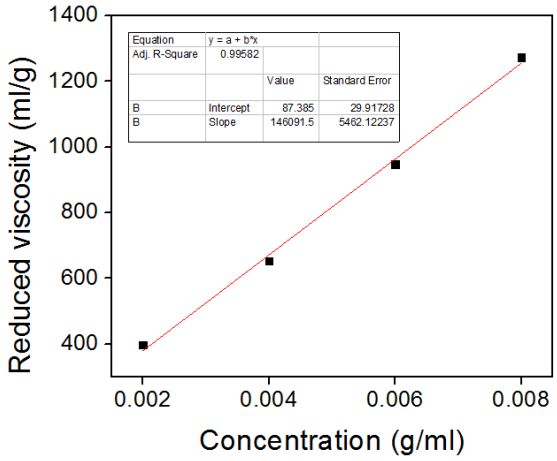

Figure 23. Lineal regression of the viscosity points as a function of the concentration in the chitosan sample.

In addition it is observed that the regression coefficient is 0.99582, which indicates that it the results complies with the Huggins equation. Applying the Mark-Honking equation (equation 3) an average molecular weight of 108,717.5 g/mol was obtained. The molecular weight

calculated is within the ranges specified in the chitosan product label (50,000-190,000 g/mol).

3.4 Thermal analysis

Through the data acquisition system a heating/cooling curve for chitosan was obtained in an air atmosphere (Figure 24), where it can be identified a phase transformation at approximately 225 °C and it is attributed to the thermal degradation of the chitosan.

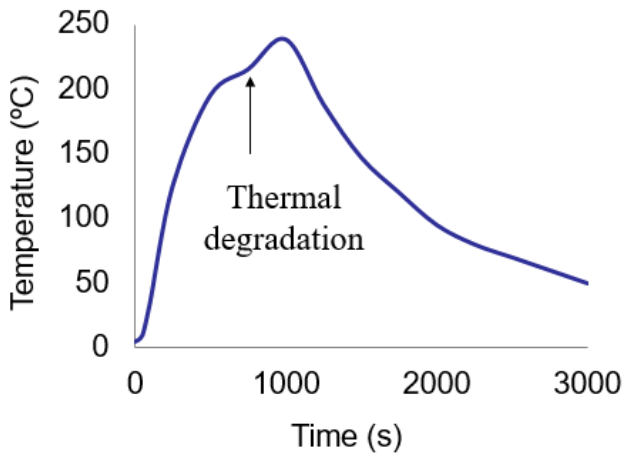

Figure 24. Heating/cooling curve for chitosan.

Figure 24 shows TG and DTG curves for chitosan, the first thermal event is observed at 56 °C, which is attributed to the loss of water (8 wt %) weakly bound to the polymeric structure.

The second thermal event is observed at 225 °C that is attributed to the degradation of the chitosan and it includes both decomposition and oxidation reactions.

In the last stage, it can be seen at 287 °C a high weight loss (50 wt%) that is attributed to a depolymerization process [44].

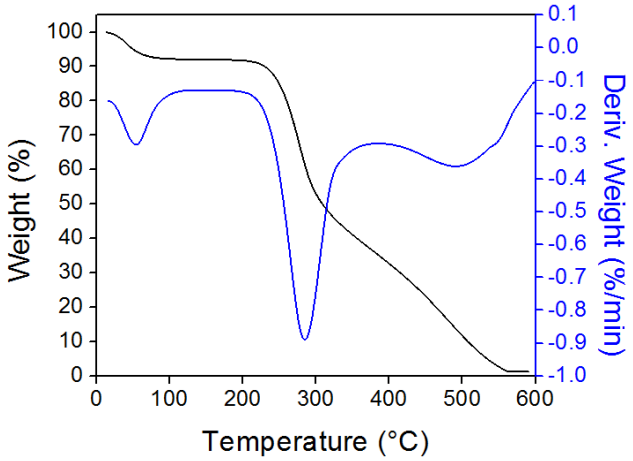

Figure 25. TG/DTG curves of chitosan.

Figure 26 demonstrated trough the TG and DTG curves of CNS that it is stable to temperatures of approximately 300 °C and a weight loss (5.3 wt %) at 54 °C that is attributed to organic residue and moisture. The weight loss of the CNS during heating to 900 °C is an additional 90.5 wt % that is attributed to the oxidation of the amorphous material first, followed by oxidation of the short-order graphitic structures above 615 °C [45].

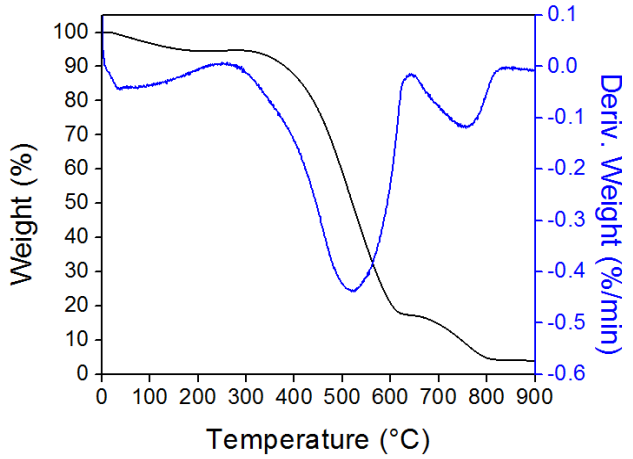

Figure 26. Thermogravimetric analysis for CNS.

Figure 27 shows the main transitions of chitosan obtained through a DSC analysis in air atmosphere, in which an endothermic transition corresponding to the loss of moisture is observed at 56 ° C, followed by an exothermic transition at 287 ° C due to the decomposition process of chitosan [44].

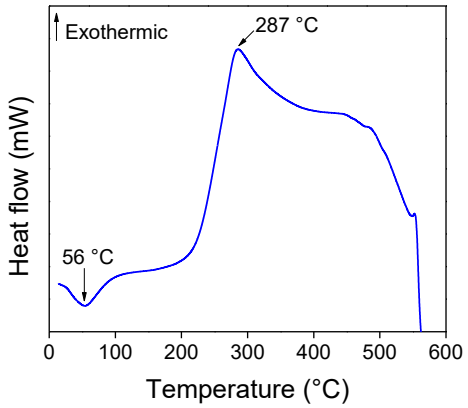

Figure 27. DSC analysis for chitosan.

3.5 Infrared spectroscopy

Figure 28 shows the FTIR spectrum of chitosan. The main absorption bands of the chitosan functional groups are described in Table 10.

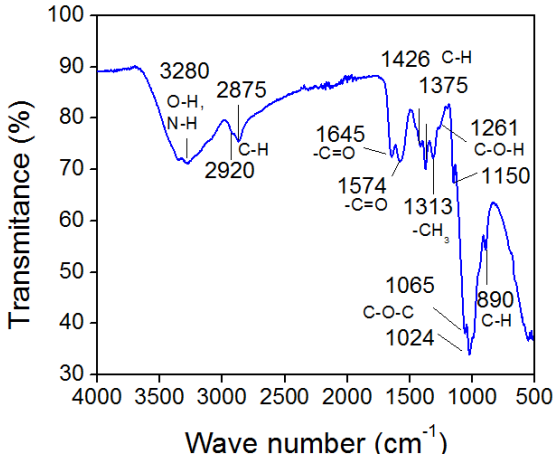

Figure 28. IR Spectrum of the chitosan.

Table 10. Main absorption bands for chitosan.

Wave number (cm^{-1})	**Absorption bands**
3750-3000	ν(O-H) overlapped to the ν_s(N-H)
2920	ν_{as}(C-H)
2875	ν_s(C-H)
1645	ν(-C=O) secondary amide
1574	ν(-C=O) protonated amide
1426, 1375	δ(C-H)
1313	ν_s(-CH_3) tertiary amide
1261	ν(C-O-H)
1150, 1065, 1024	ν_{as}(C-O-C) and ν_s(C-O-C)
890	ω(C-H)

Figure 29 shows the absorption spectrum in terms of absorbance, through equation 8, a value of 82.81% was obtained, which corresponds to that specified in the product label (75-85%).

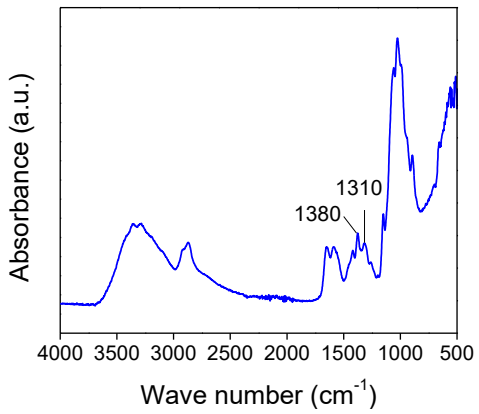

Figure 29. FTIR spectrum of chitosan (absorbance units).

Figure 30 shows the FTIR spectra of chitosan after heating above its thermal degradation temperature (230 °C) for 30 min and 60 min in air atmosphere. The spectral changes are clearly seen, indicating the degradation of the polymer as a consequence of its heating. The decrease of the intensities of the band at 3280 cm^{-1} is attributed to dehydration due to the loss of the oxhidrile groups, at 1645 and 1580 cm^{-1} is observed the loss of the acetyl and amino groups and the decrease of the intensities at 2932, 2867 and all under 1420 cm^{-1} are attributed to depolymerization reactions [46].

All this indicates that sintering above the thermal degradation temperature causes negative effects in the synthesis of the composite, due to the loss of the main functional groups of chitosan.

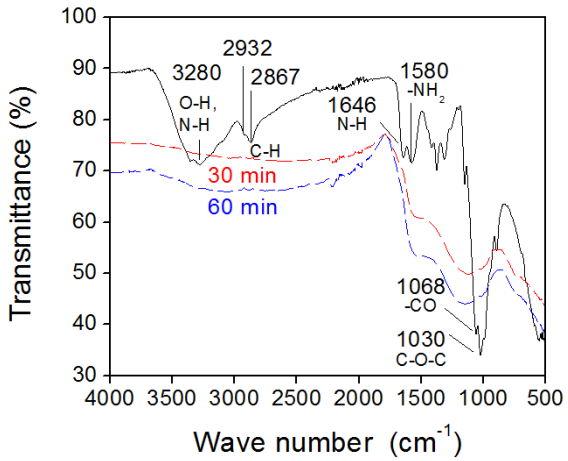

Figure 30. Infrared spectra of a chitosan before and after heating it 280 °C for 30 min and 60 min.

In order to identify the possible interaction between chitosan and CNS, FTIR spectra form the chitosan-CNS composites were obtained. Chitosan can be linked to the CNS through the hydroxyl, amino and acetyl groups of the molecule.

Figure 31 shows that the increase of intensities of O-H and N-H absorption bands (red arrows) compared with the control samples and a slight shift to the right show a possible interaction of the CNS by the oxhidrile group, as well as the increase of the intensity at 1580 cm^{-1} (blue arrows) corresponding to an interaction by the amino group and the increase of intensities at 2932, 2867 (black circles) and the intensity around 1313 cm^{-1} (black arrows) demonstrate an interaction with acetyl groups [47]. It can be seen in Figure 31b. that bonding with all main functional groups of chitosan are favored when composites are sintered for 5 h and 220 °C, as compared to those sintered at 120 ° C which are favored only by the hydroxyl and acetyl groups.

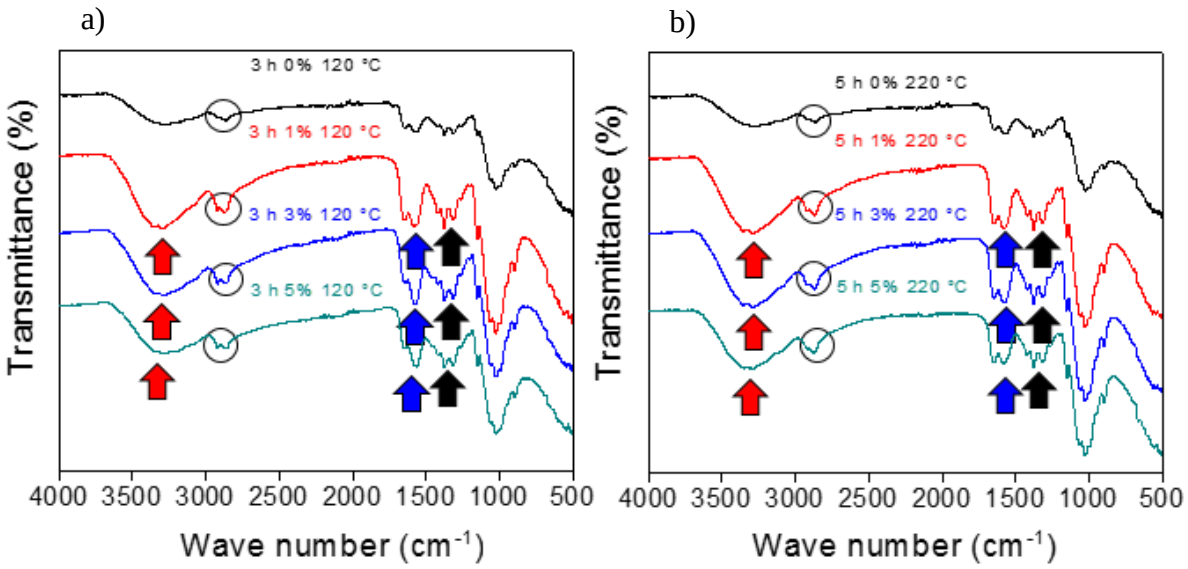

Figure 31. FTIR spectra of chitosan-CNS sintered for: a) 3 h at 120 °C and b) 5 h at 220 °C.

Another way of identifying possible interactions of chitosan functional groups is by the shifting of some vibration bands. Figure 32 shows that the peak at 1645 cm^{-1} corresponding to the secondary amine group and the small band at 1587 cm-1 assigned to N-H and amide groups of chitosan exhibit a slight shift to the right, suggesting that some amino groups were converted into amide groups and the interaction between the chitosan and CNS [47].

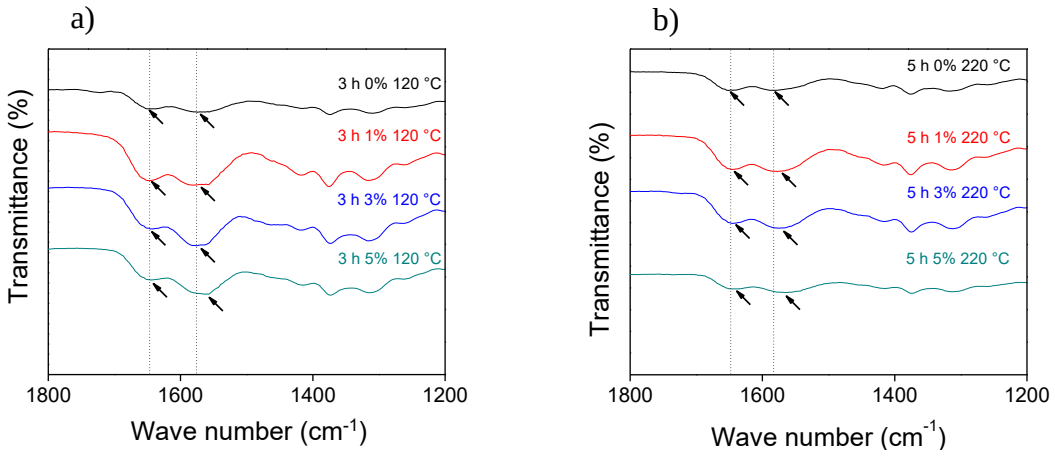

Figure 32. FTIR spectra of chitosan-CNS sintered for: a) 3 h at 120 °C and b) 5 h at 220 °C.

3.6 Raman spectroscopy

Figure 33 shows the main absorption Raman bands of chitosan which are described in Table 11.

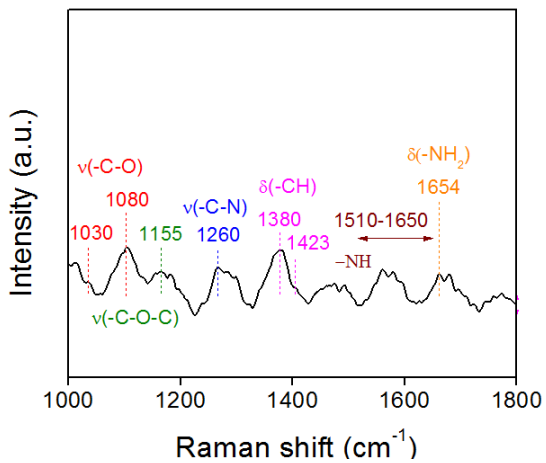

Figure 33. Raman spectrum of the chitosan.

Table 11. Main absorption Raman bands for chitosan.

Wave number (cm^{-1})	**Absorption bands**
1654	Bond doubling $-NH_2$
1598	Vibrational bonding doubles N-H
1380, 1423	Alkane C-H Bends
1155	Antisymmetric stretches of the C-O-C bridge
1030, 1080	Vibrations involving C-O stretching

Figure 34 shows the Raman spectra of raw and milled CNS; the two main signals correspond to the D (1366 cm^{-1}) and G (1597 cm^{-1}) bands that are typical of graphitic carbon [48].

The D band is caused by disordered structure of graphene and it is observed in sp2 hybridized carbon systems, in the other hand, G band rises from the stretching of the C-C bond in graphitic materials, and is common to all sp2 carbon systems. Raw CNS Raman spectrum shows one second-order combinational of fullerene C_{60} identified at 2860 cm^{-1} (Ag(2)+Hg(7)) [48]. When CNS are milled, the intensity of the fullerene C_{60} decreased due to its fragmentation and the increasing intensity of the 2D band in the milled CNS spectrum by the formation of graphene after milling, 2D band is a secondary peak and it means the largest intensity in single layer graphene [48].

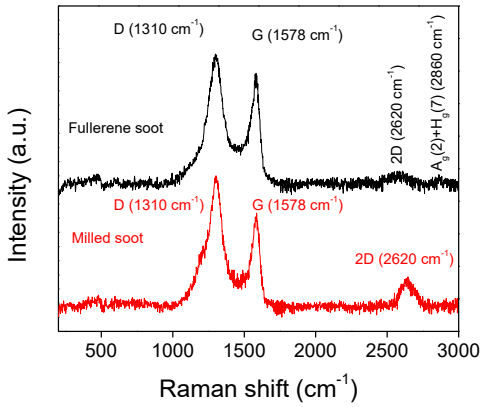

Figure 34. Raman spectra of CNS with and without milling.

Figure 35Figure 36 show the Raman spectra of the control samples and the chitosan-CNS conducted at 100x and 1000x magnifications respectively. Using a 100x magnification, Raman active bands of chitosan can be identified by the vibration of the C-O stretching at 1080 and 1030 cm^{-1} that corresponds to the saccharide structure of chitosan, as well as the antisymmetric stretches of the C-O-C bridge at 1155 cm^{-1}, C–H bending at approximately 1380 and 1423 cm^{-1} and the N–H bending found at 1598 cm^{-1} and corresponds to the primary amine group [49].

When the analysis is conducted to at 1000x, a higher spatial resolution analysis is obtained and it allows the identification of the graphitic carbon Raman bands in the chitosan-CNS composites. Spatial resolution is determined by a combination of the laser spot size and the spacing between acquisition points on the sample and is a function of the objective magnification and the laser wavelength (higher magnification and shorter wavelengths produce smaller spot sizes) [50].

The presence of CNS in the chitosan matrix is identified by the G and D bands how are the most common bands of carbon, implying that they are located at the surface of the chitosan particles making proper interaction within in the composite.

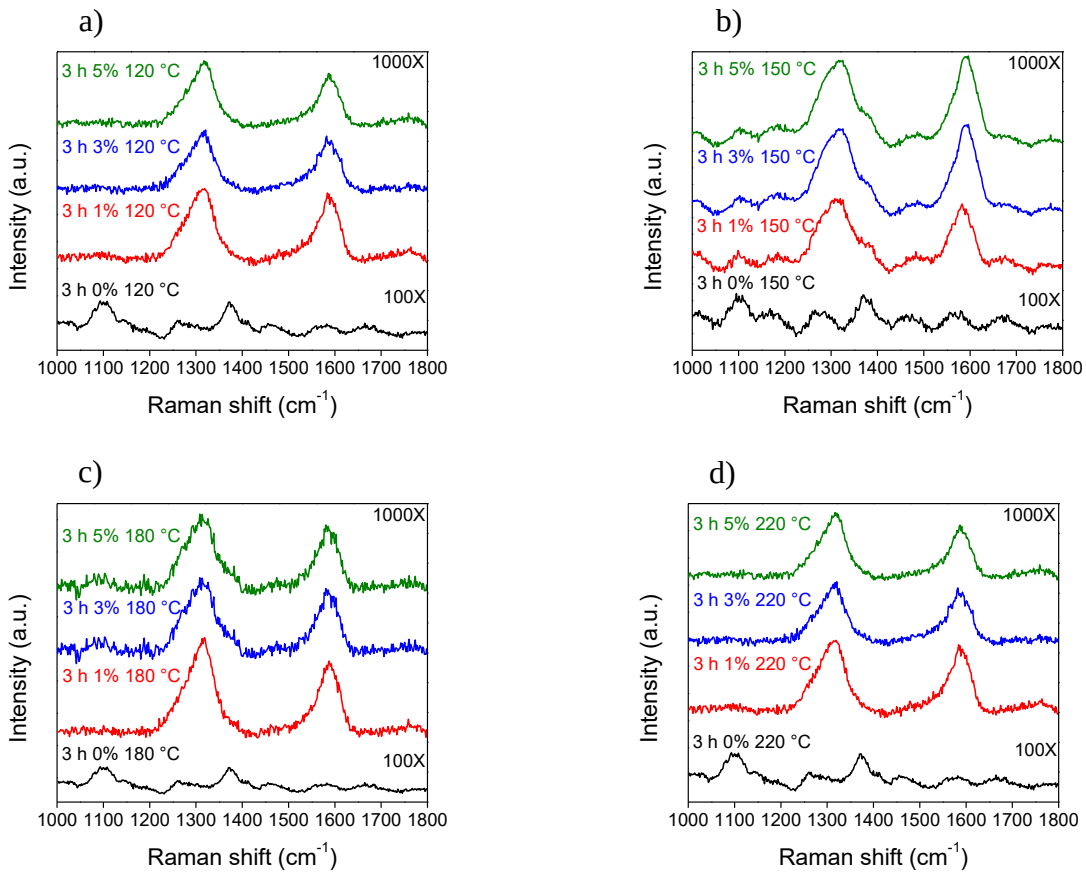

Figure 35. Raman analysis for chitosan-CNS composites sintered for 3 h at: a) 120, b) 150, c) 180 and d) 220 °C.

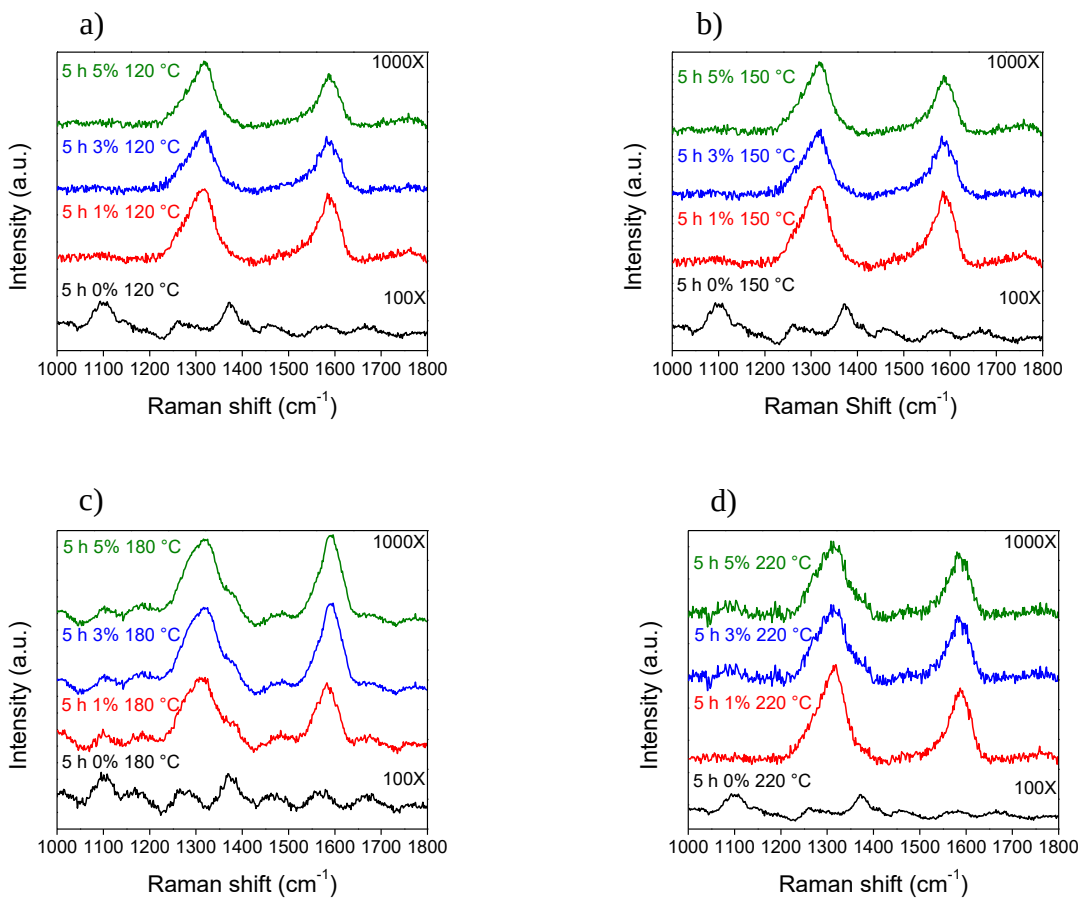

Figure 36. Raman analysis for chitosan-CNS composites sintered for 5 h at: a) 120, b) 150, c) 180 and d) 220 °C.

3.7 X-ray diffraction

Figure 37 shows that the X-ray diffraction pattern of chitosan consists of an amorphous and a crystalline part, reveling that chitosan is a semi-crystalline material. Chitosan has two main characteristic peaks at 2θ = 10 ° and 20 °which consist of the α-chitin and a crystal β-chitin phases, respectively [38]. α-chitin has a structure of antiparallel chains while β-chitosan has intrasheet hydrogen-bonding by parallel chains [51].

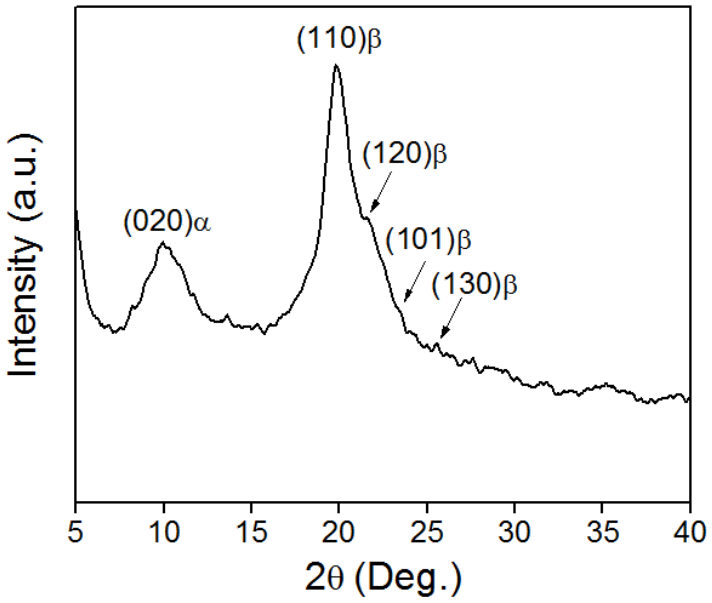

Figure 37. X-ray diffractogram of chitosan.

By means of the Focher equation (equation 10) it was possible to determine that the chitosan has an index of crystallinity of 58.27%.

Figure 38a shows the XRD patterns of the samples of chitosan at different milling times. As can be seen in Figure 38b, as the milling time increases, the characteristic peaks of chitosan tend to widen and decrease their intensities, thus causing a reduction in their crystallinity index due to micro deformations in the crystal lattice of the material produced as a consequence high energy ball milling [52].

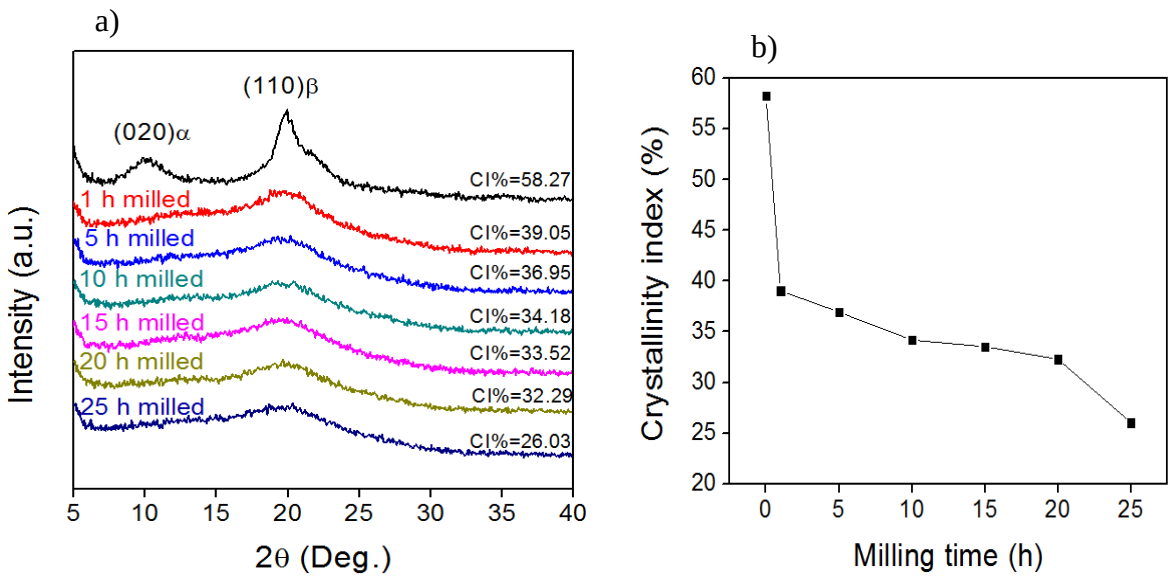

Figure 38. a) XRD analysis of chitosan at different milling time and b) Crystallinity index analysis at different milling time.

Figure 39 presents the XRD pattern of raw and milled CNS. Raw CNS show a low intensity pattern with a well-defined peak corresponding to the plane (002) and the presence of fullerene C_{60}. XRD pattern of milled CNS showing that the plane (002) diffraction suffers an amorphization due the mechanical milling and the presence of the graphene characteristic peaks by the fragmentation of the fullerene [48].

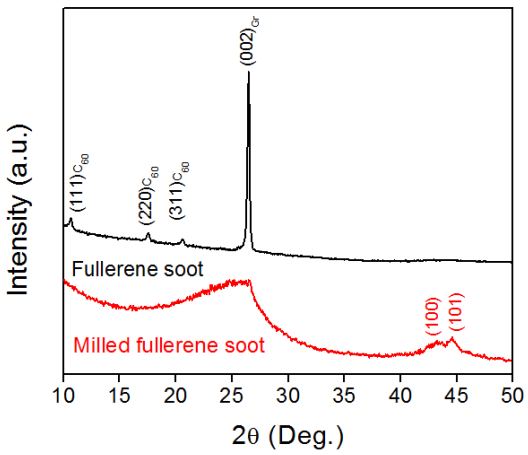

Figure 39. X-ray diffractograms of CNS with and without milling.

Figure 40 and Figure 41 show the diffraction patterns of the chitosan-CNS composites sintered for 3 h at different sintering temperatures. The α-chitin and β-chitin phases are present in each of the diffractograms as well as the characteristic peak of the deflexion of the (002) plane of amorphous graphite.

When reinforcer is added to the matrix and the sintering temperature increases, the main characteristic peaks of the chitosan begin to widen and the intensities of these same ones begin to decrease, this phenomenon and with the presence of the α-chitin and β-chitin phases in the chitosan-CNS composites it is known the crystalline structure is not changed but the crystallinity index tends to decrease.

One reason of the decreasing crystallinity index may be due to a kind of intermolecular reaction between CNS and chitosan, which causes that the greater the amount of reinforcer will cause the molecular chains of chitosan more difficulty to move [53]. The effects of the sintering temperature shows that the higher these conditions, the greater the mobility of the chitosan polymer chains, which indicates that there is low molecular ordering by the chains.

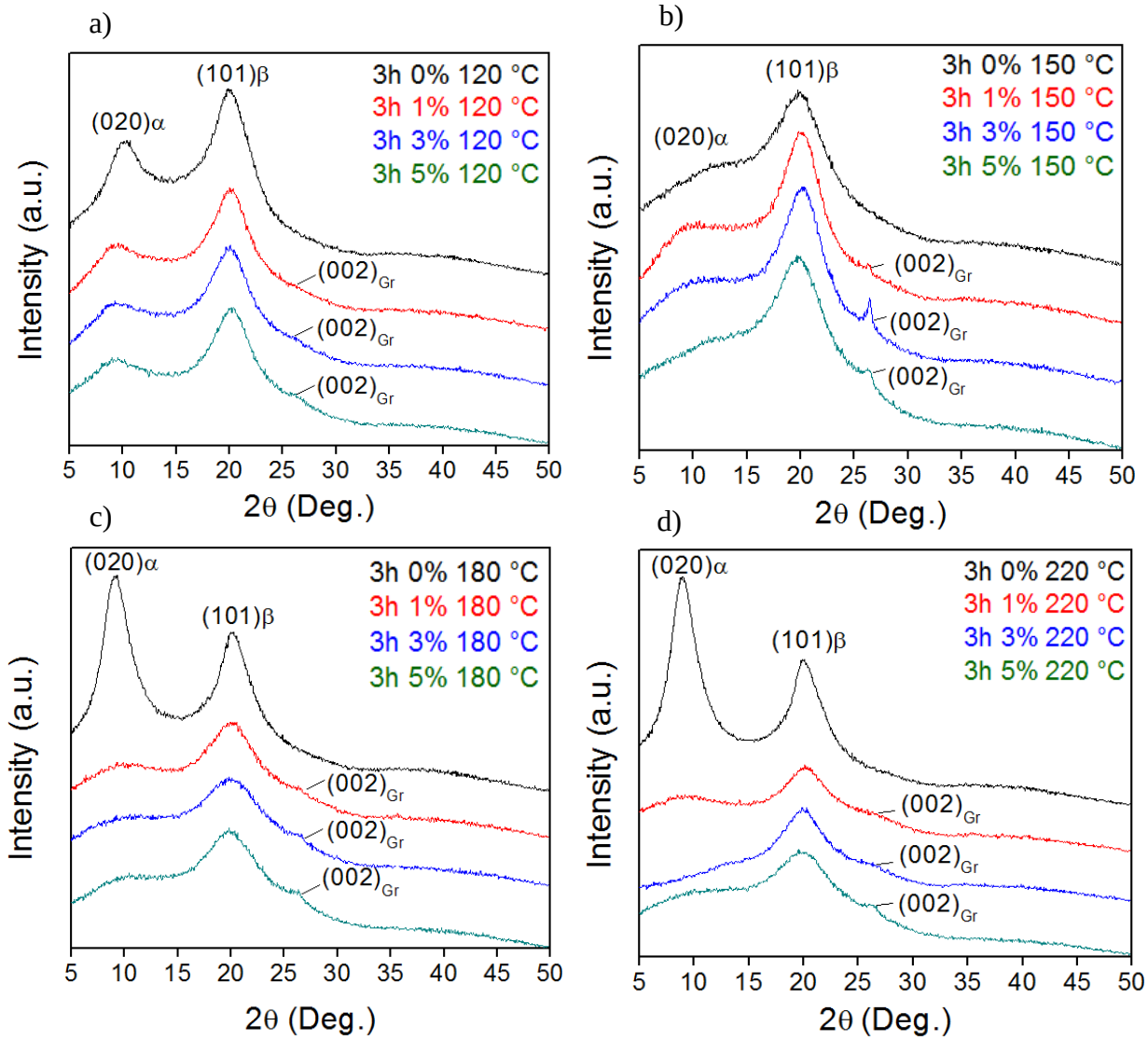

Figure 40. XRD results of Chitosan-CNS composites sintered for 3 h at: a) 120, b) 150, c) 180 and d) 220 °C.

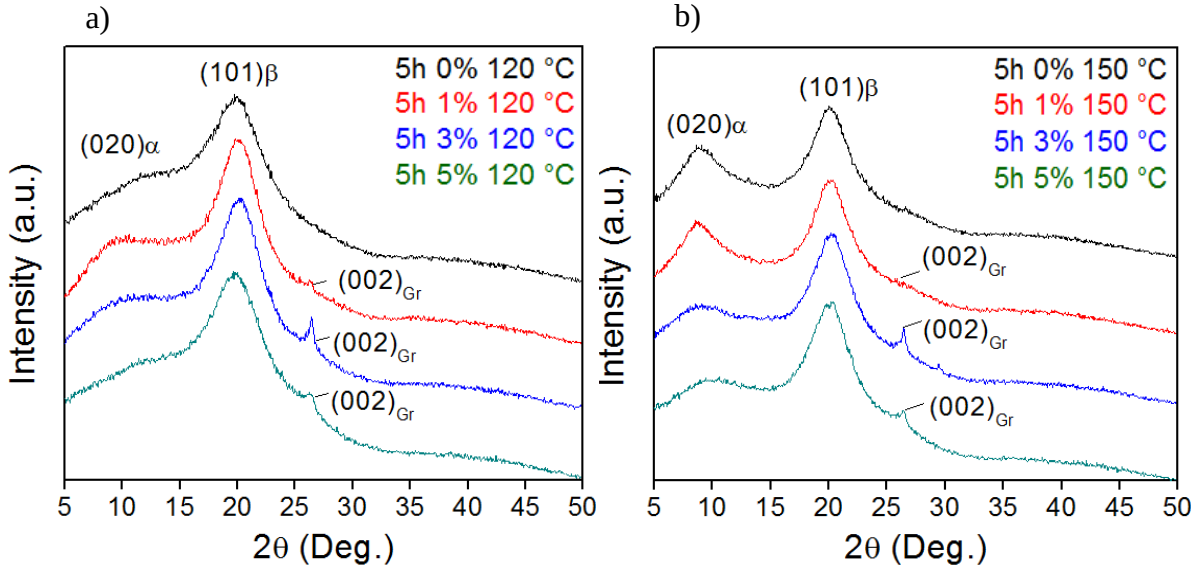

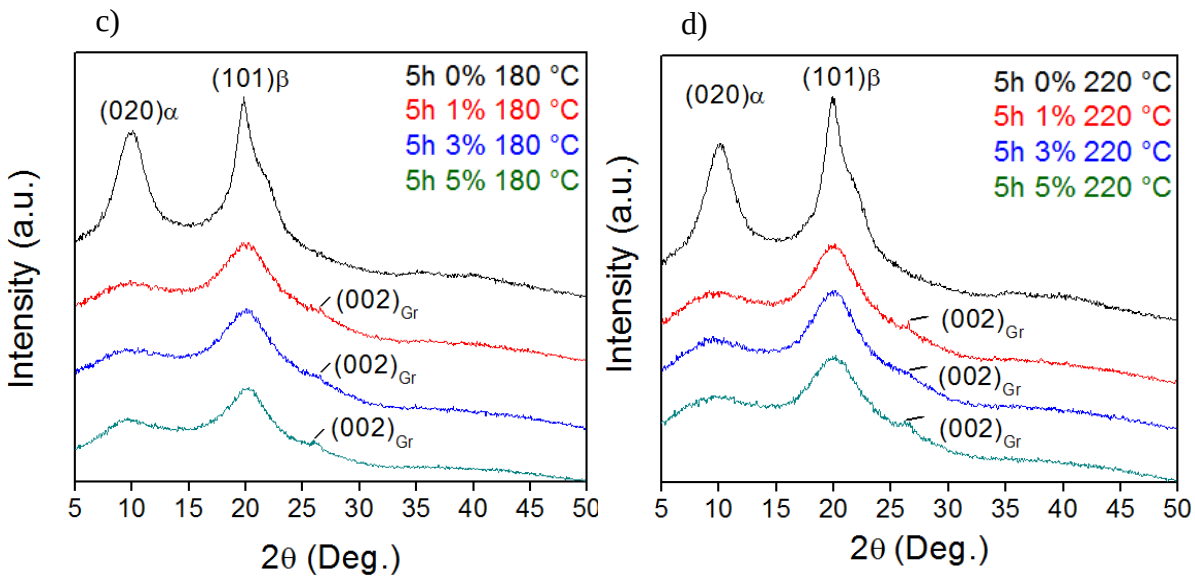

Figure 41. XRD results of chitosan-CNS composites sintered for 5 h at: a) 120, b) 150, c) 180 and d) 220 °C.

Figure 42 shows the results of crystallinity index using the Focher equation (equations10 and 11). It is possible to observe how the crystallinity index gradually decreases as the sintering conditions increase and the addition of reinforcer in the matrix increases. However, the biggest contributors are the temperature and sintering time.

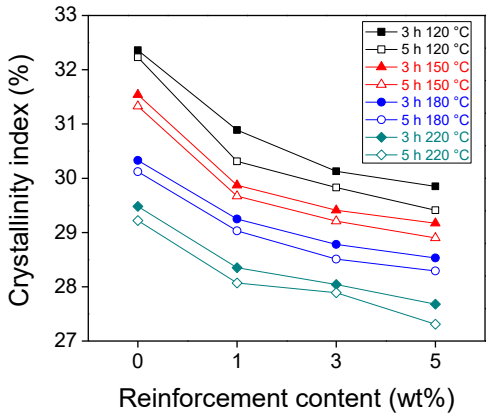

Figure 42. Variation of crystallinity with sintering conditions.

3.8 Density

Figure 43 shows the density results of the chitosan-CNS composites. According to the data sheet of the product, chitosan has a bulk density of 0.15-0.30 g/cm^3, while fullerene soot has been reported to have a density of ~1.7 g/cm^3 [54]. Since the density of these CNS are higher than chitosan, the addition of CNS leads to an increase in the density of the material as long as the reinforcer is uniformly distributed in the matrix.

The results in Figure 43a. shows that sintering at 180 °C exhibits a consistent behavior in the increase of the density with the addition of reinforcer. In Figure 43b. this same behavior is observed for every sintering temperature (unless at 120 °C, that has a density decrease from an incorporation of the 3 wt% of reinforcer) but the highest densities are obtained when chitosan-CNS composites are sintered at 150 °C for 5 h.

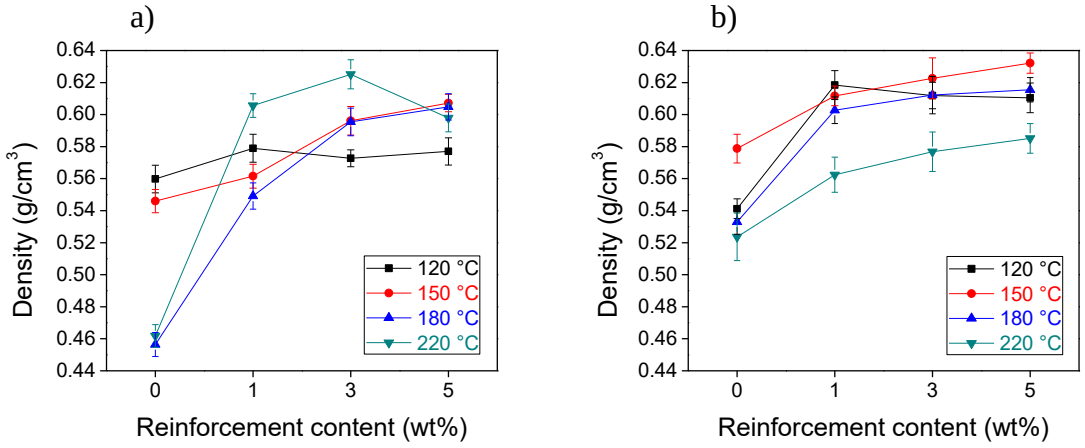

Figure 43. Density results of chitosan-CNS composites sintered for: a) 3 h and b) 5 h.

3.9 Porosity

Figure 44 shows the porosity results, both cases demonstrated that sintering temperature is the major factor contibuyent of the pore reduction, especially when is working with 180 °C, which demonstrate that at 3 and 5 h of sintering the lower porosity is obtained.

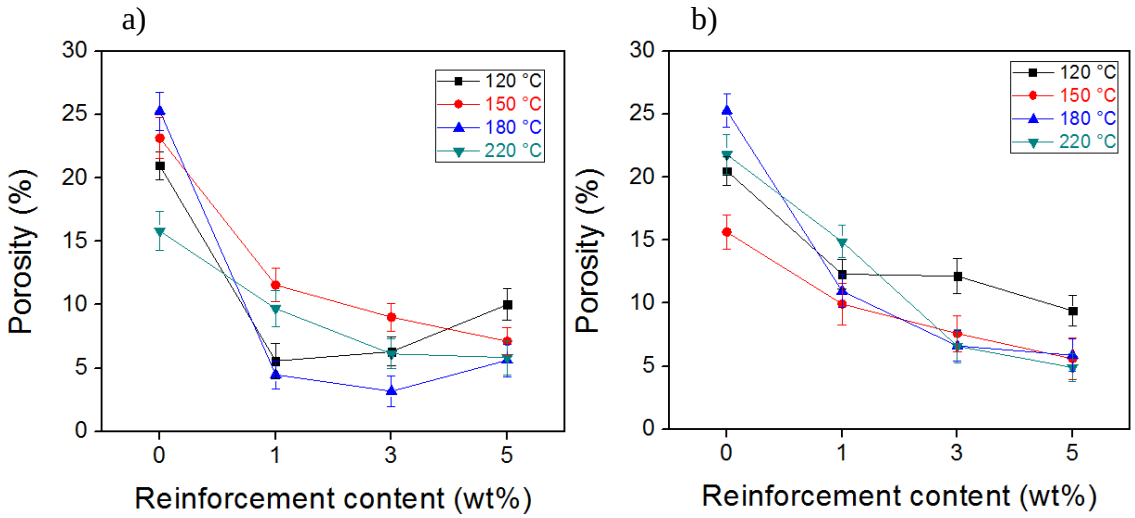

Figure 44. Porosity results of chitosan-CNS composites sintered for: a) 3 h and b) 5 h.

3.10 Scanning electron microscopy

Figure 45 show the SEM micrographs of raw chitosan at different magnifications, at high magnifications (Figure 45a.) it can be seen that chitosan has a solid morphology with a regular distribution of particles of different sizes. At higher magnifications (Figure 45b.) chitosan fibers can be observed.

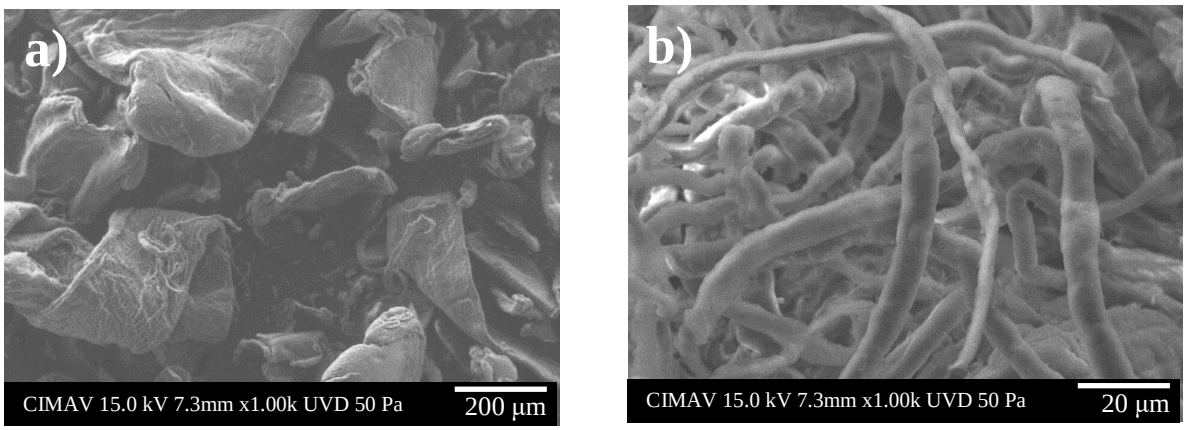

Figure 45. SEM micrographs of chitosan at a) 500 and b) 1000x.

Figure 46 shows the morphology of the milled chitosan at different milling time, when chitosan is milled for 1 h (see Figure 46a.) a regular distribution of particles is obtained but there is no good homogeneity in the particle size. On the other hand milling chitosan for 5 h (see Figure 46b.) gives a better distribution and a homogenization in the particle size.

With the increase of the milling time (Figure 46c, d, e and f) particles starts to form agglomerates, which it indicates that high milling times does not improves comminution of the material and can be attributed by effect of cold welding or mechanical interaction due to the constant fragmentation of the material [55].

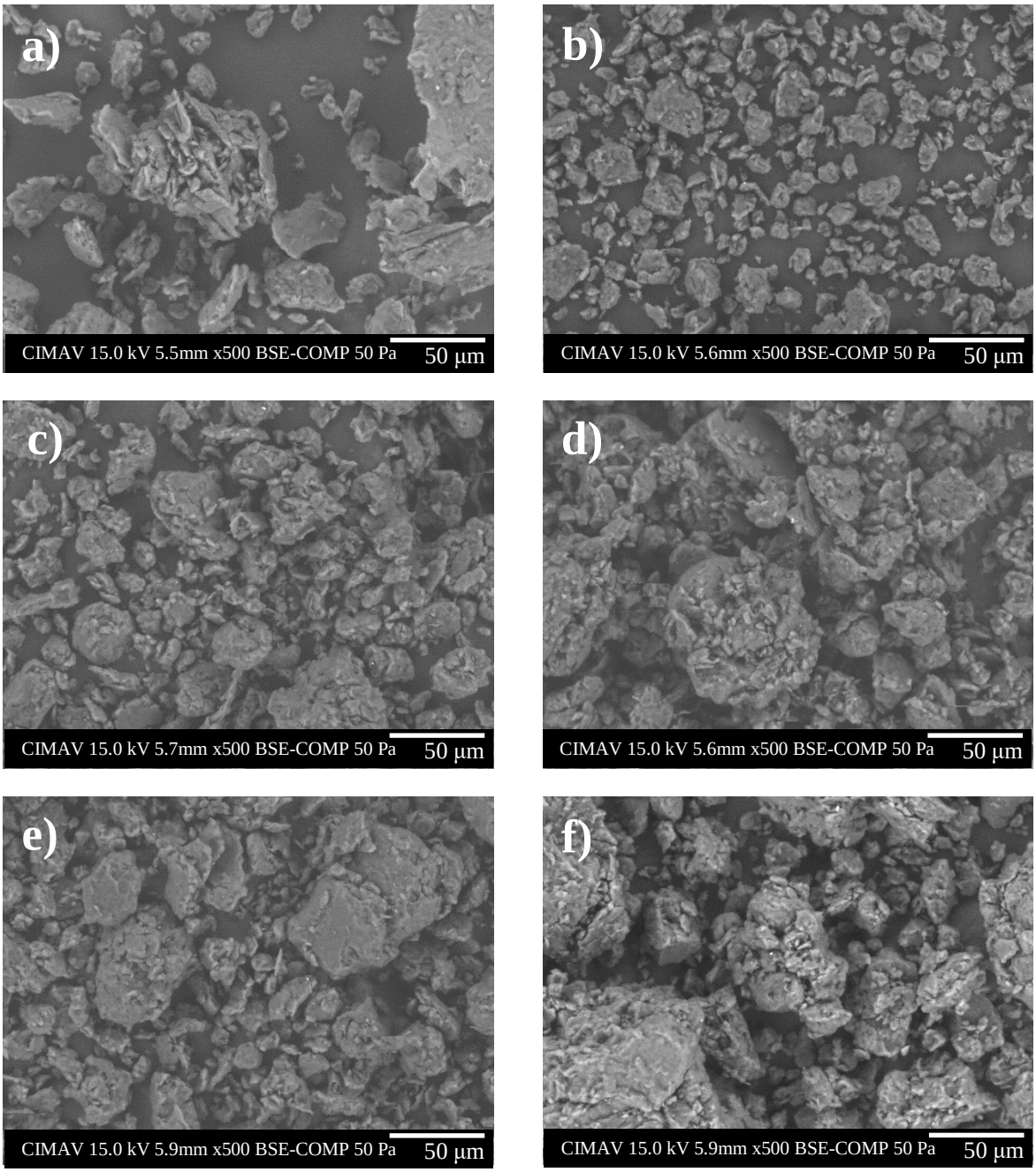

Figure 46. SEM micrographs of chitosan milled for a) 1, b) 5, c) 10, d) 15, e) 20 and f) 25 h.

The micrograph of CNS shown in Figure 47a presents a fluffy appearance. When CNS are milled it loses this morphology and starts to consolidate into particles with a more defined shape (see Figure 47b).

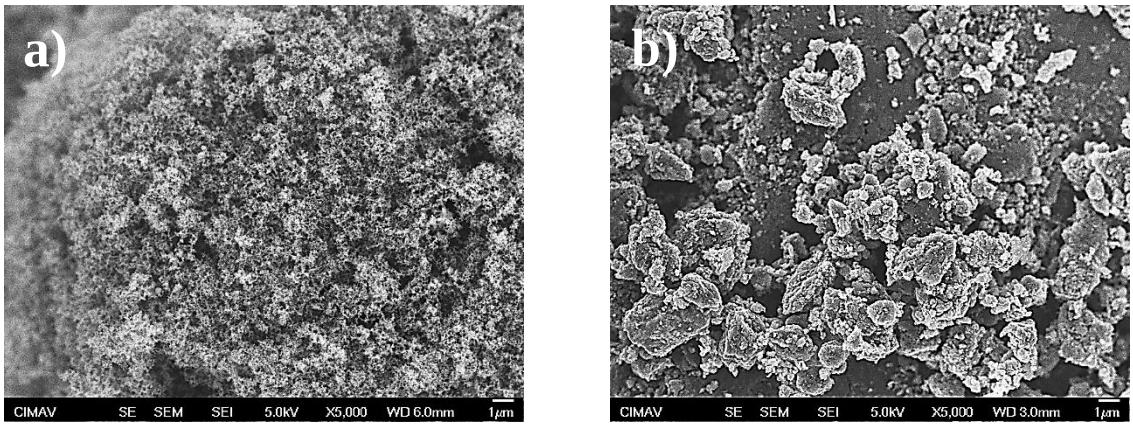

Figure 47. SEM micrographs of: a) CNS and b) Milled CNS.

Figure 48 shows the micrographs of ground powders of chitosan and CNS once milled together for 1 h, the powders agglomerate into clusters that are carbon coated along their surface.

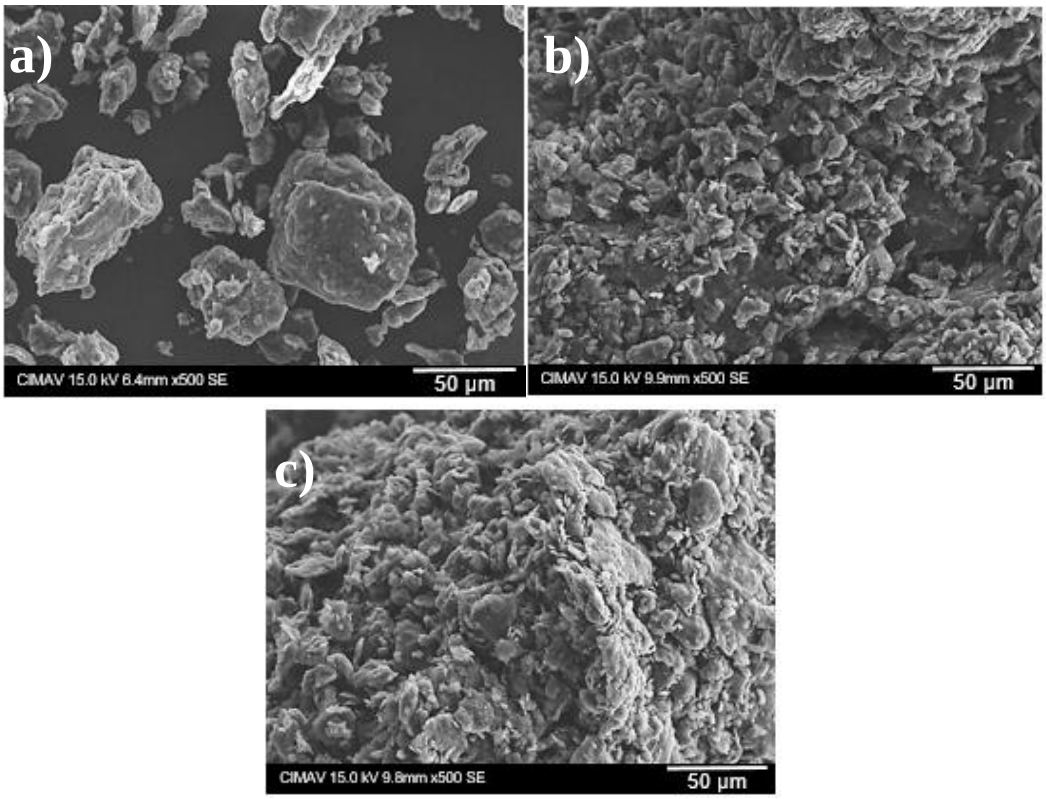

Figure 48. SEM micrographs of milled chitosan powders mixed with: a) 1 wt%, b) 3 wt% and c) 5 wt% of milled CNS.

Figure 49 shows the surface morphology of the control samples, which shows that at 3 and 5 h of sintering there is little consolidation between the chitosan particles, but this is slightly improved with increasing temperature and sintering time.

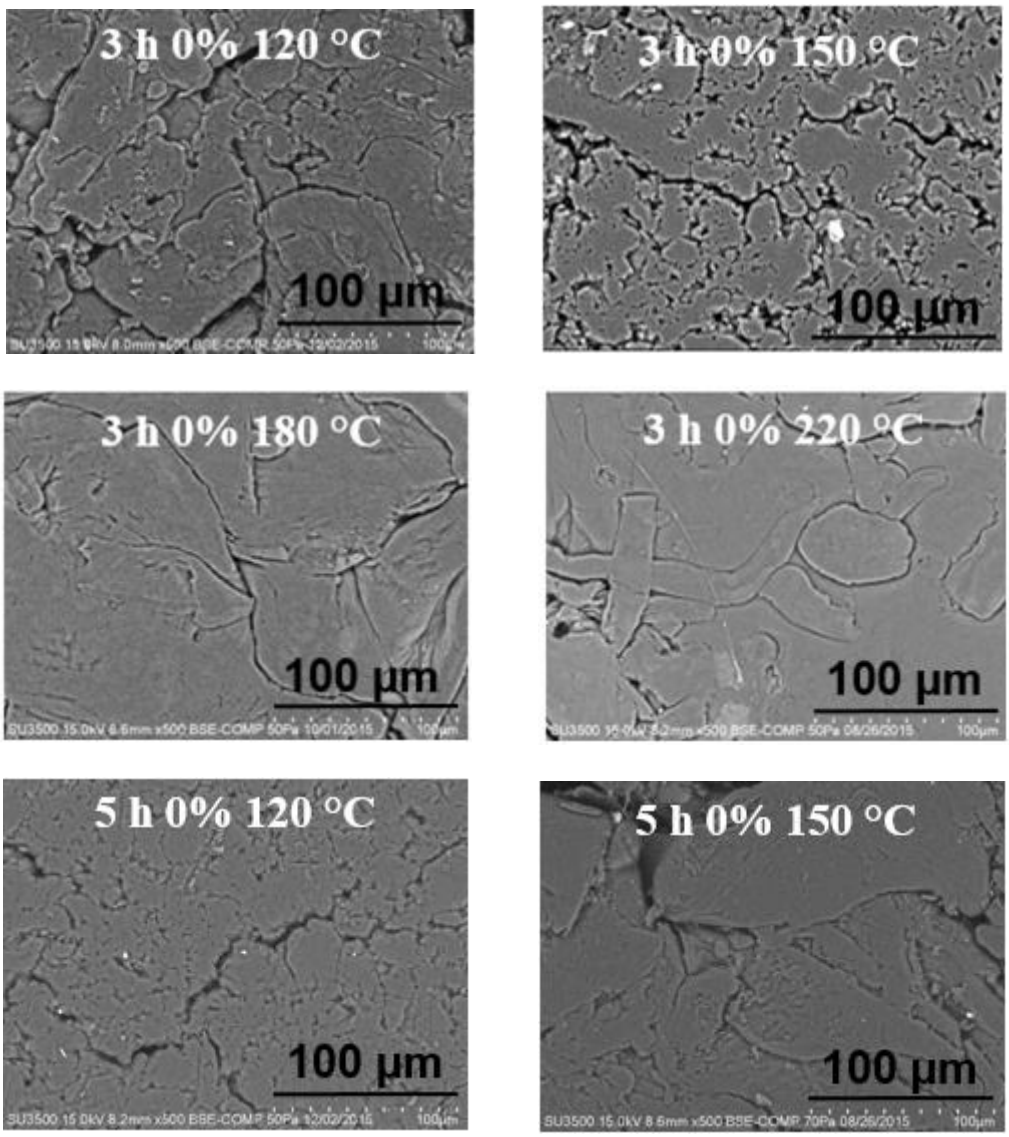

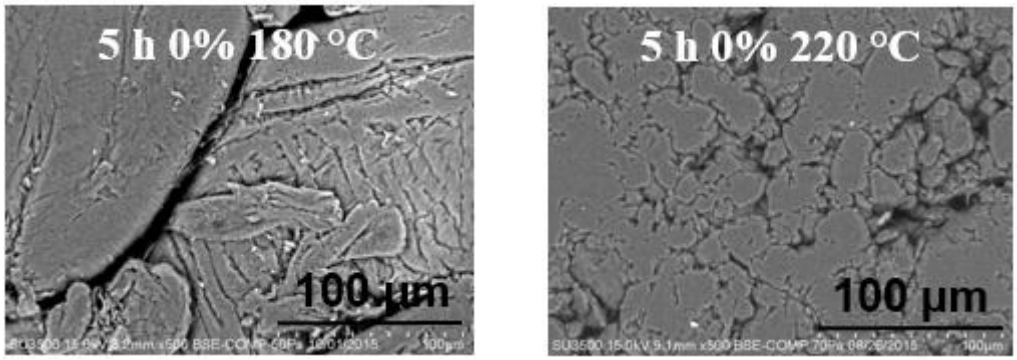

Figure 49. SEM micrograph of control samples.

On the other hand, in Figure 50 it can be observed that there is a better consolidation between the chitosan and the CNS as the sintering conditions increase, where a reduction in the porosity and a better union between the components of the composite is achieved.

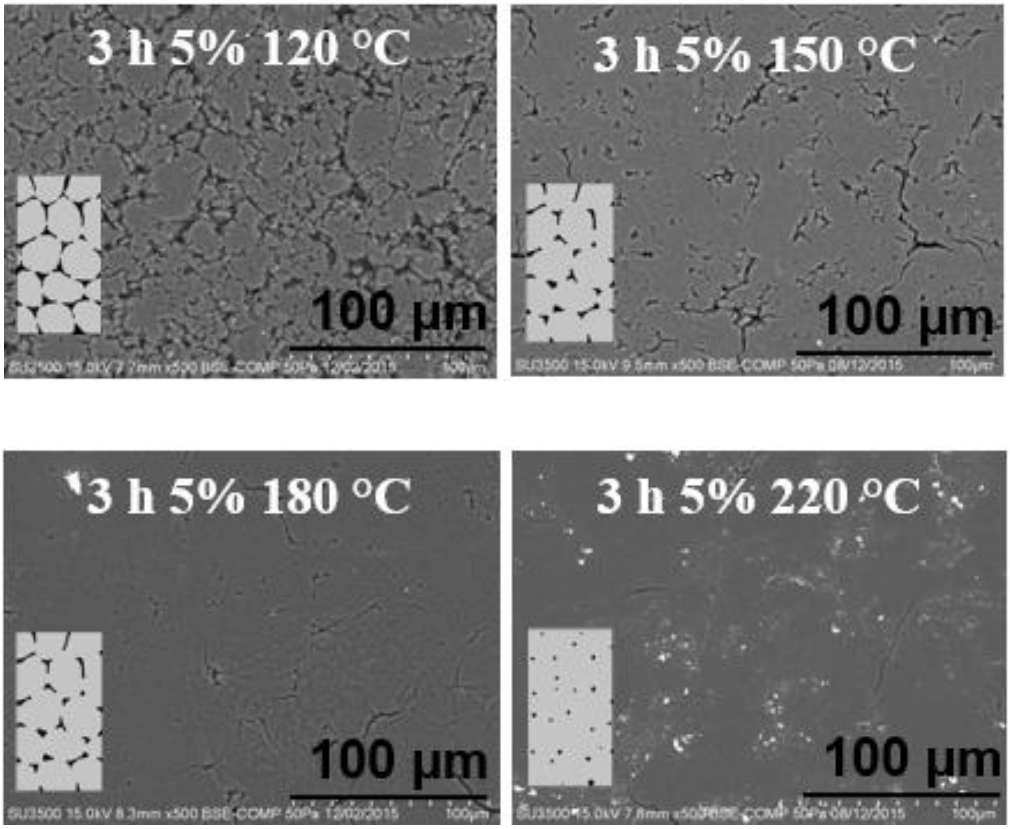

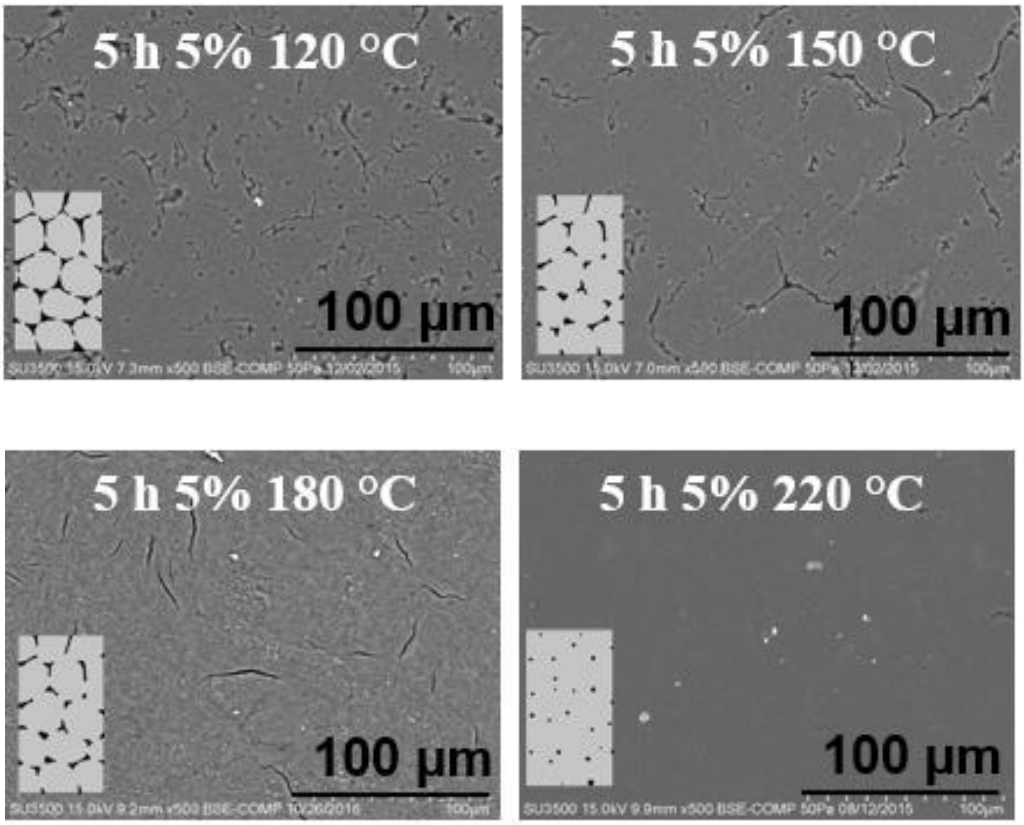

Figure 50. SEM micrographs of representative chitosan-CNS composite samples.

3.11 Transmission electron microscopy

Figure 51 shows a TEM micrograph of the CNS where it reveals that is formed consists of nanostructured particles of approximately 50 nm in size ordered at short range.

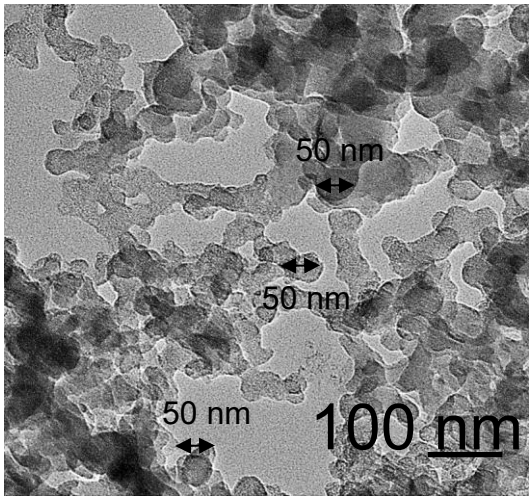

Figure 51. TEM micrograph of CNS.

Figure 52 shows the TEM micrograph of the sample milled CNS. With 3 h milling time sponsor further cold welding of the graphene layers, transforming it into graphitic structures with up to 5 graphene layers [56].

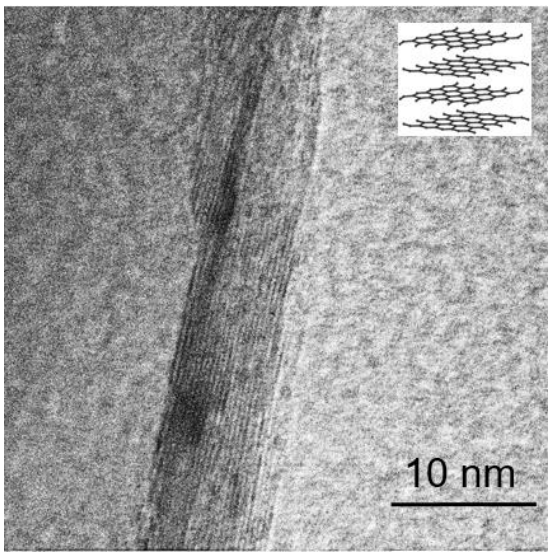

Figure 52. TEM micrograph of milled CNS.

Figure 53 shows the TEM micrograph of a representative chitosan-CNS composite sample (3h 5% 180 °C). This figure shows the interface between the CNS and the chitosan, where CNS have graphitic nature having an interatomic distance of 0.35 nm.

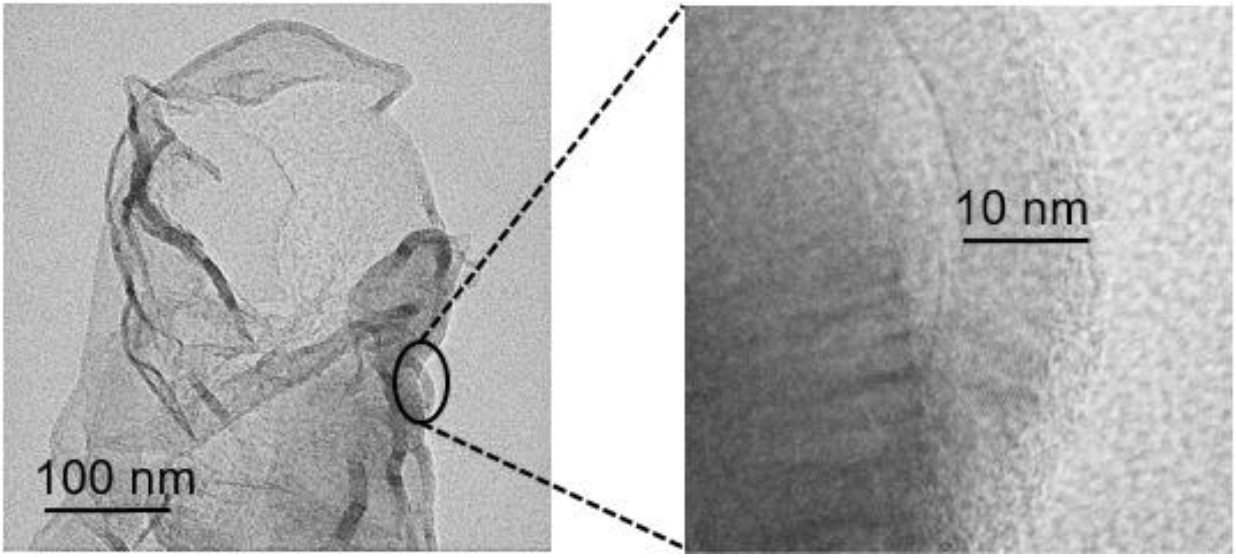

Figure 53. TEM micrograph of a representative chitosan-CNS composite sample.

3.12 Microhardness Vickers

Figure 54 shows the results of Vickers microhardness, where the lowest hardness is shown when the composites are sintered at 120 ° C but this hardness improves as the sintering temperature increases and the addition of reinforcer to the matrix. When comparing the results of 3 and 5 h of sintering, it can be observed that the values are very close to each other, so that the sintering time has little influence on the improvement of microhardness. It is evident that the microhardness of the composites that are sintered at high temperatures increases because at these temperatures a greater contraction of pore and a better consolidation of the components is achieved, which favors the bond between particles and makes it more resistant, permitting obtain a material with greater hardness.

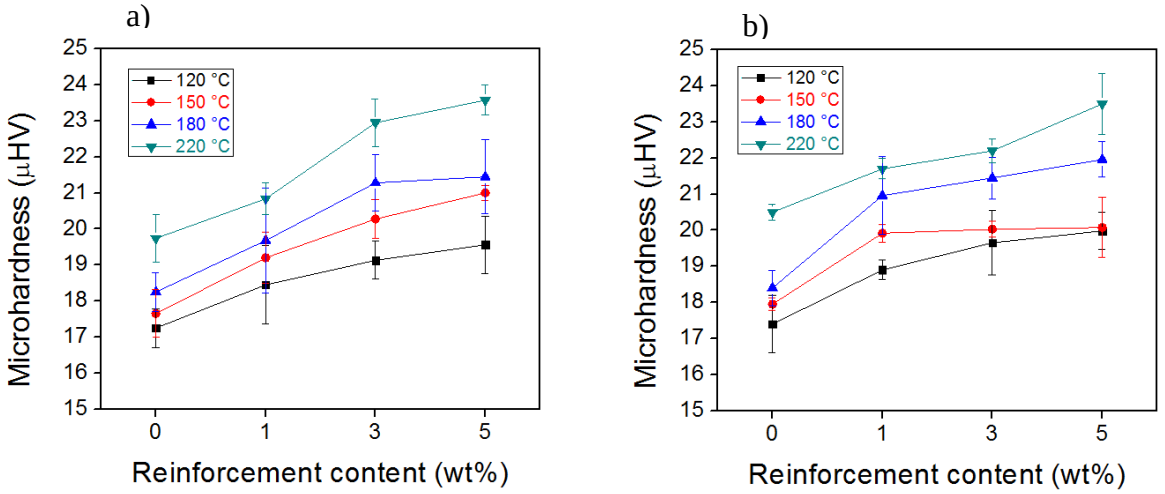

Figure 54. Microhardness testing of the chitosan-CNS composites sintered for: a) 3 h and b) 5 h.

From the results shown in the Figure 54, it was observed that the highest hardness was obtained at 180 and 220 ° C, through an ANOVA analysis (Appendix A.1) and a Tukey test, it was determined that there is no significant difference between sintering at 180 and 220 ° C, as well as sintered at 3 and 5 h, whereby it is concluded that the best sintering conditions are at 3 h, at 180 ° C with 5 wt% of reinforcer.

Table 12 shows the Vickers microhardness results reported by different methods. According to the sample previously selected (3 h 5% 180 °C) a 45% improvement of Vickers microhardness is obtained when compared with chitosan films and 10% when chitosan is reinforced with carbon nanotubes (solution evaporation method).

Table 12. Vickers microhardness results reported by diverse methods.

Method	Reinforcement content	Vickers microhardness
Chitosan films [57]	0 wt%	12 μHV
Solution evaporation [26]	1 wt%	20 μHV
Uncross-linked [27]	2 wt%	23 μHV

3.13 Nanoindentation test

The load curve corresponds to an elastoplastic deformation, characterized by the elastoplastic properties of the material, whereas the curve corresponding to the discharge generally represents a pure elastic behavior, which indicates that after discharge all the elastic displacements they are recovering. As can be observed in Figure 55, the control samples show a very low elastic recovery, indicating that the material behaves rigidly, as the amount of reinforcer increases the load curve displacement is greater and more important greater elastic recovery.

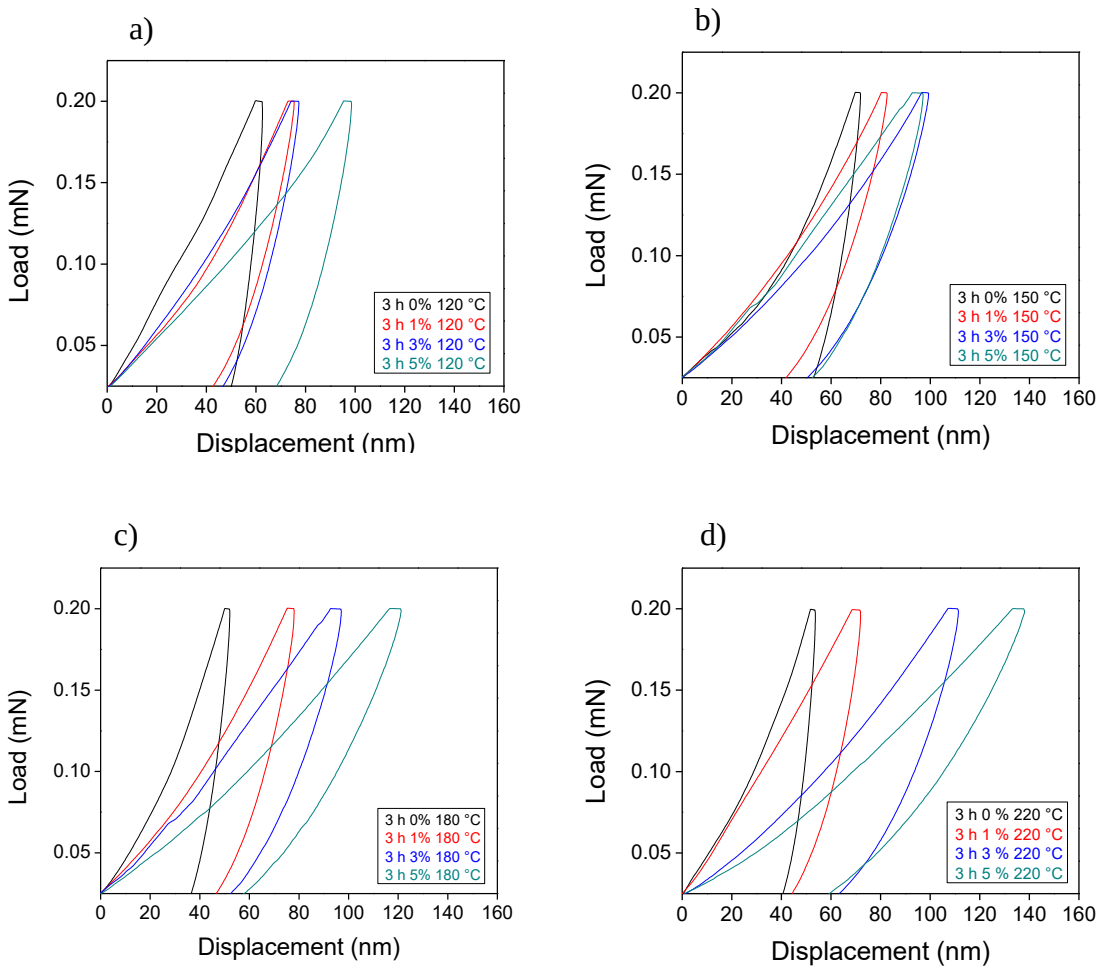

Figure 55. Load-displacement curves for chitosan-CNS composites sintered for 3 h at: a) 120, b) 150, c) 180 and d) 220 °C.

Figure 56 shows the same phenomena when chitosan-CNS are sintered for 5 h, showing a greater elastic recovery by the addition of reinforcer and when chitosan-CNS are sintered at 180 and 220 ° C.

The elastic behavior of the composite with the incorporation of CNS can be attributed to the elastic behavior of the graphical nature of the CNS interface with chitosan. The single layer had reported outstanding elastic behavior [58] and self-healing mechanisms numerically [59] and experimentally [60].

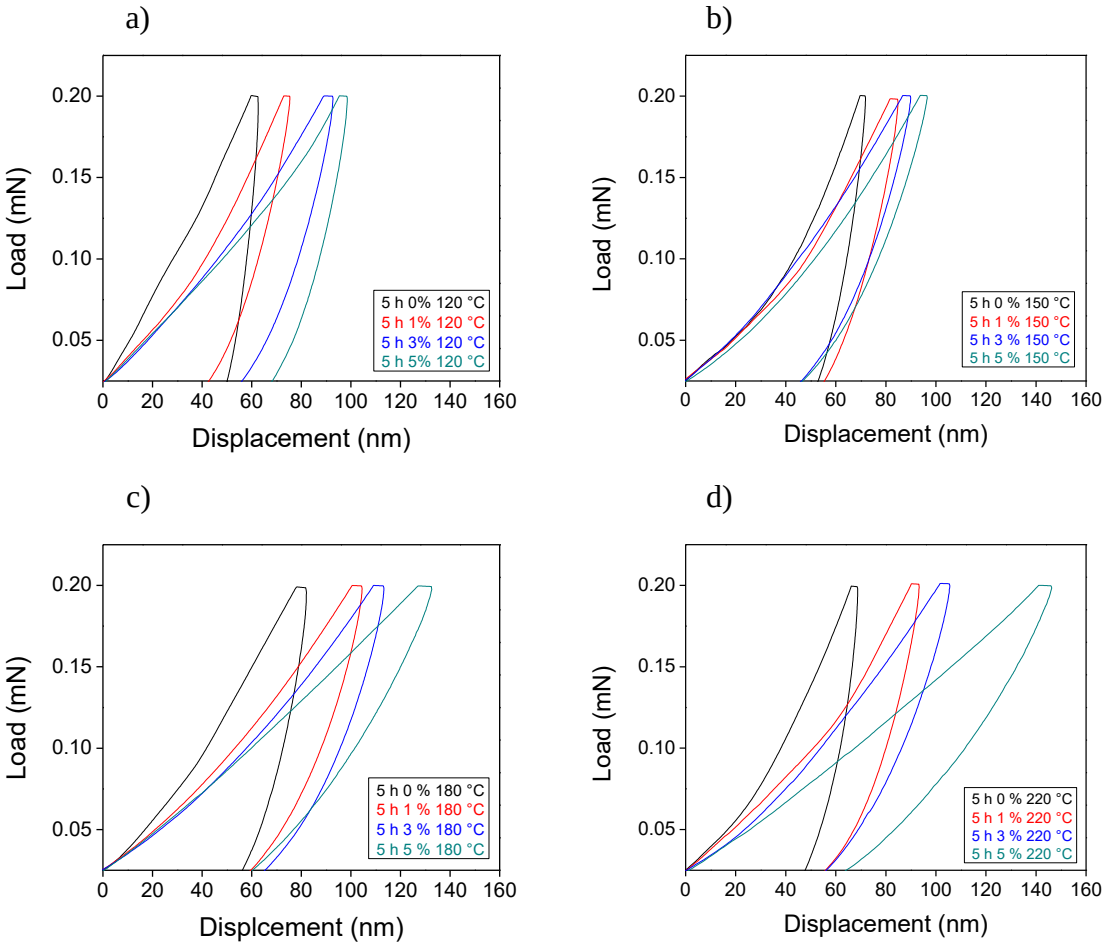

Figure 56. Load-displacement curves for chitosan-CNS composites sintered for 5 h at: a) 120, b) 150, c) 180 and d) 220 °C.

The obtained results are translated into values of elastic modulus and they can be seen in Figure 57, where the modulus E is related to the rigidity of the material, reason why a low value of modulus E indicates that the material behaves more elastically.

Figure 57a shows that the lowest modulus E is obtained when chitosan-CNS composite is sintered at 180 °C with an incorporation of 5 wt% of reinforcer, which means that a more elastic material is obtained under these conditions.

According to the sintering conditions, at high temperature and sintering time a decrease in the index of crystallinity is observed. As crystallinity increases in a polymer, the stiffness increases. When the crystallinity index is lowered, the material allows to behave more elastically because the chains are less defined in the material, causing them to be easily moved.

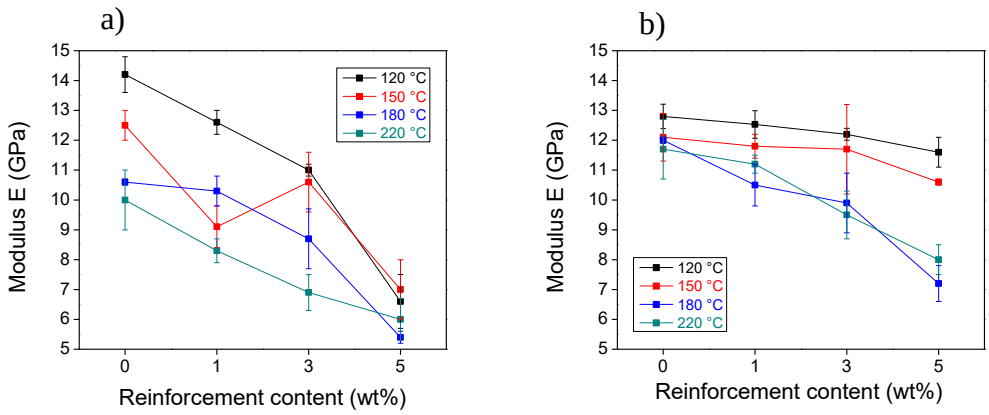

Figure 57. Elastic modulus of chitosan-CNS composites sintered for: a) 3 and b) 5 h.

Through an ANOVA analysis and a Tukey test (Appendix A.2), it was determined that there is no significant difference between sintering at 180 and 220 ° C wit 5 wt% of reinforcer (which gives the lowest values of modulus E), but when is compared between 3 and 5 h the analysis show that there is a significate difference, however since the lowest modulus E is sought, 3 h of sintering was selected at 180 °C.

Table 13 shows the results obtained by means of other synthesis techniques, compared with 3 h 5% 180 °C composite, a 92 and 21 % of elastic modulus is achieved when is compared with chitosan films and uncross-linked methods, respectively.

Table 13. Elastic modulus results reported by diverse methods.

Method	**Reinforcement content**	**Modulus E**
Chitosan films [61]	0 wt%	65 GPa
Uncross-linked [27]	2 wt%	7 Gpa

Figure 58 shows the results of nanohardness for the chitosan and chitosan–CNS composites. It can be seen that the nanohardness increases slightly with the addition of reinforcer to the matrix, but the increase of the sintering temperature contributes to the improvement of the nanohardness due to with the increase of sintering temperature, partial coalescence happened, and a higher value for hardness [62]. As well as the improvement of density and integrity of the components.

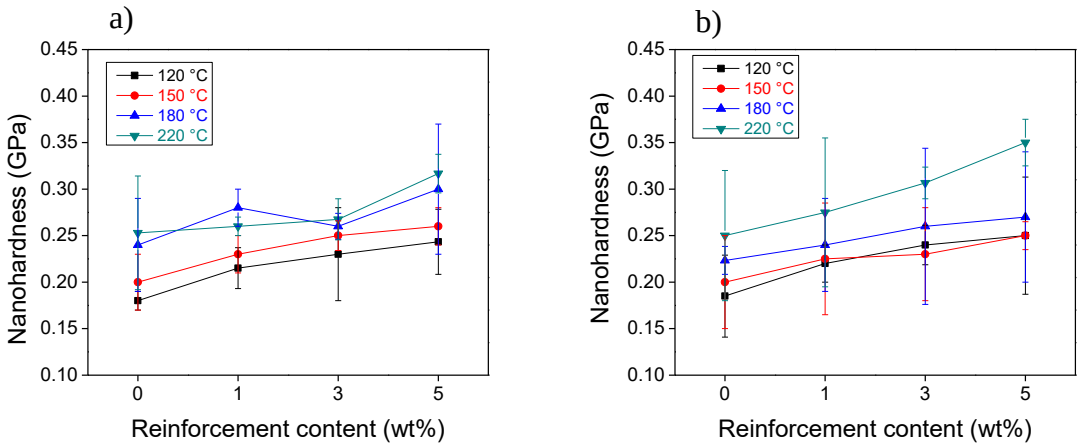

Figure 58. Nanohardness of chitosan-CNS composites sintered for: a) 3 and b) 5 h.

ANOVA analysis and Tukey tests (Appendix A.3) show that there is no significate difference when chitosan-CNS composites are sintered with 5 wt% of reinforcer at 120, 150, 180 and 220 °C, even sintering for 3 and 5 h there is no significate difference, which it means that at nanoscale the composite does not seem to have significant improvement on nanohardness, however 3 h of sintering at 180 °C with 5 wt% of reinforcer is still selected.

Table 14 shows the nanohardness results reported by different methods. When these are compared with the sample 3 h 5% 180 °C, an improvement of 70% in nanohardness is obtained when compared with chitosan films and 35% when compared with uncross-linked method.

Table 14. Nanohardness results reported by diverse methods.

Method	Reinforcement content	Nanohardness
Chitosan films [63]	0 wt%	0.08 GPa
Cross linked [27]	2 wt%	0.18 Gpa

3.14 Optical microscopy

Figure 59 Figure 60 show optical micrographs of chitosan–CNS composites. In the chitosan samples the grain boundaries are wider than those in the sintered samples. This results from the expected low cohesion among the chitosan particles that is improved with the sintering conditions and the addition of CNS. In the following micrographs, it is possible to visualize the grain boundary and the effect of temperature in the chitosan–CNS composite. The arrows in Figure 59 Figure 60 are used to indicate the grain boundary.

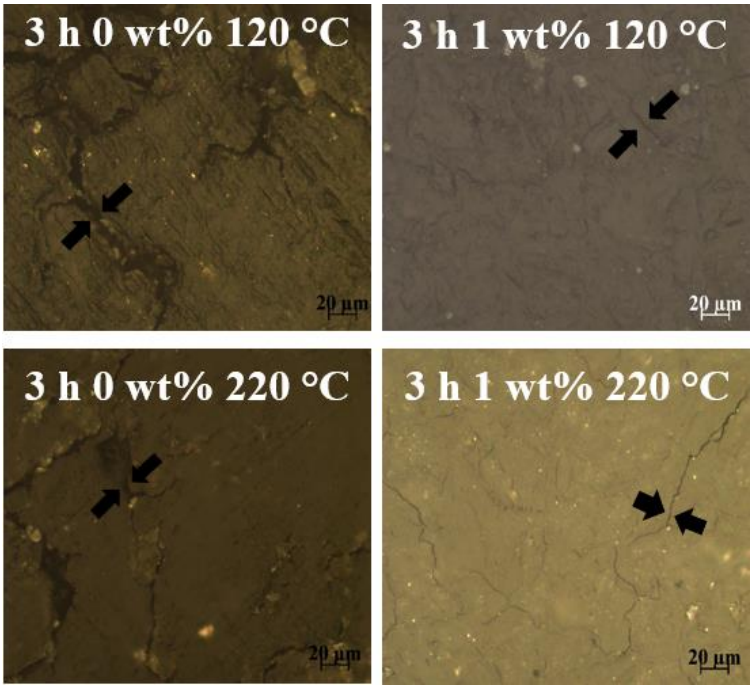

Figure 59. Optical characterization of representative chitosan-CNS composites samples sintered for 3 h.

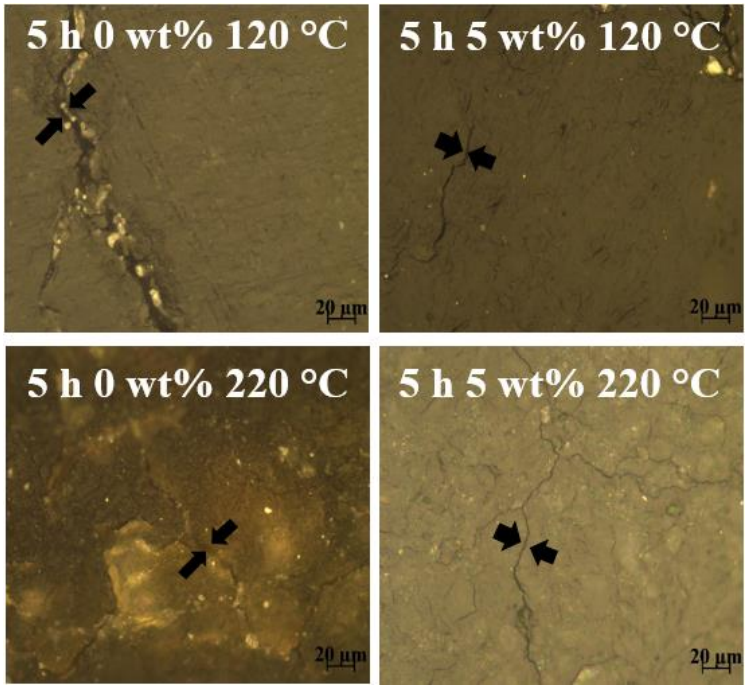

Figure 60. Optical characterization of representative chitosan-CNS composites samples sintered for 5 h.

CHAPTER 4:

CONCLUSIONS AND FUTURE WORK

4.1 Conclusions

- In this work, it was shown that it is possible to prepare chitosan-CNS composites by a thermomechanical process involving mechanical milling and conventional sintering.
- A refined grain structure of the chitosan and a homogeneous dispersion of CNS are obtained by mechanical milling.
- The thermal degradation temperature was determined successfully by thermal analysis, which contributed to optimize the sintering temperatures of the material.
- Temperature improves the sintering effectiveness by reducing grain boundaries and porosity that in turn results in better intimacy among the constituents in the composite.
- The optimum conditions are obtained when chitosan is milled for 5 h and composites are sintered for 3 h at 180 ° C with 5 wt% CNS, obtaining an improvement in micro and nanohardness of 16 and 18%, respectively, and an improvement in elastic behavior of 52% when compared to the control sample.

4.2 Future work

- Carry out a detailed analysis using transmission electron microscopy to evaluate the interface between the matrix and the reinforcing phase.
- To evaluate the mechanical properties of the composites by macroscopic tests.
- Determine the pore size of composites for future applications.

APPENDIX

APPENDIX A.1 ANOVA analysis for Vickers microhardness results.

One Way ANOVA

Overall ANOVA

	DF	Sum of Squares	Mean Square	F Value	Prob>F
Model	3	28.90821	9.63607	31.63729	8.70255E-5
Error	8	2.43664	0.30458		
Total	11	31.34484			

Null Hypothesis: The means of all levels are equal
Alternative Hypothesis: The means of one or more levels are different
At the 0.05 level, the population means are significantly different.

Fit Statistics

R-Square	Coeff Var	Root MSE	Data Mean
0.92226	0.02534	0.55189	21.77625

Means Comparisons

Tukey Test

	MeanDiff	SEM	q Value	Prob	Alpha	Sig	LCL	UCL
150 °C 120 °C	1.1	0.45061	3.45226	0.14587	0.01	0	-0.87674	3.07674
180 °C 120 °C	3.21	0.45061	10.07431	4.5536E-4	0.01	1	1.23326	5.18674
180 °C 150 °C	2.11	0.45061	6.62205	0.00685	0.01	1	0.13326	4.08674
220 °C 120 °C	3.835	0.45061	12.03582	1.28927E-4	0.01	1	1.85826	5.81174
220 °C 150 °C	2.735	0.45061	8.58356	0.00135	0.01	1	0.75826	4.71174
220 °C 180 °C	0.625	0.45061	1.96151	0.53993	0.01	0	-1.35174	2.60174

Sig equals 1 indicates that the means difference is significant at the 0.01 level.
Sig equals 0 indicates that the means difference is not significant at the 0.01 level.

ANOVA analysis between samples with 5 wt% CNS sintered for 3 h at different sintering temperature

One Way ANOVA

Overall ANOVA

	DF	Sum of Squares	Mean Square	F Value	Prob>F
Model	3	11.7825	3.9275	7.93434	0.0088
Error	8	3.96	0.495		
Total	11	15.7425			

Null Hypothesis: The means of all levels are equal
Alternative Hypothesis: The means of one or more levels are different
At the 0.05 level, the population means are significantly different.

Fit Statistics

R-Square	Coeff Var	Root MSE	Data Mean
0.74845	0.06717	0.70356	10.475

Means Comparisons

Tukey Test

	MeanDiff	SEM	q Value	Prob	Alpha	Sig	LCL	UCL
150 °C 120 °C	-0.5	0.57446	1.23091	0.81989	0.01	0	-3.02	2.02
180 °C 120 °C	-2.2	0.57446	5.41603	0.02096	0.01	1	-4.72	0.32
180 °C 150 °C	-1.7	0.57446	4.18511	0.07045	0.01	1	-4.22	0.82
220 °C 120 °C	-2.2	0.57446	5.41603	0.02096	0.01	1	-4.72	0.32
220 °C 150 °C	-1.7	0.57446	4.18511	0.07045	0.01	1	-4.22	0.82
220 °C 180 °C	0	0.57446	0	1	0.01	0	-2.52	2.52

Sig equals 1 indicates that the means difference is significant at the 0.01 level.
Sig equals 0 indicates that the means difference is not significant at the 0.01 level.

ANOVA analysis between samples with 5 wt% CNS sintered for 5 h at different sintering temperature

One Way ANOVA

Overall ANOVA

	DF	Sum of Squares	Mean Square	F Value	Prob>F
Model	1	2.83594	2.83594	6.42886	0.06429
Error	4	1.7645	0.44113		
Total	5	4.60044			

Null Hypothesis: The means of all levels are equal
Alternative Hypothesis: The means of one or more levels are different
At the 0.05 level, the population means are not significantly different.

Fit Statistics

R-Square	Coeff Var	Root MSE	Data Mean
0.61645	0.02902	0.66417	22.8875

Means Comparisons

Tukey Test

	MeanDiff	SEM	q Value	Prob	Alpha	Sig	LCL	UCL
5 h 3 h	-1.375	0.5423	3.58577	0.06429	0.01	0	-3.87205	1.12205

Sig equals 1 indicates that the means difference is significant at the 0.01 level.
Sig equals 0 indicates that the means difference is not significant at the 0.01 level.

ANOVA analysis between samples with 5 wt% CNS sintered at 180 °C at different sintering time

APPENDIX A.2 ANOVA analysis for elastic modulus results.

One Way ANOVA

Overall ANOVA

	DF	Sum of Squares	Mean Square	F Value	Prob>F
Model	3	27.42	9.14	18.18905	6.2318E-4
Error	8	4.02	0.5025		
Total	11	31.44			

Null Hypothesis: The means of all levels are equal
Alternative Hypothesis: The means of one or more levels are different
At the 0.05 level, the population means are significantly different.

Fit Statistics

R-Square	Coeff Var	Root MSE	Data Mean
0.87214	0.09088	0.70887	7.8

Means Comparisons

Tukey Test

	MeanDiff	SEM	q Value	Prob	Alpha	Sig	LCL	UCL
150 °C 120 °C	-1.7	0.57879	4.15376	0.07269	0.01	0	-4.23902	0.83902
180 °C 120 °C	-3.1	0.57879	7.57451	0.00302	0.01	1	-5.63902	-0.56098
180 °C 150 °C	-1.4	0.57879	3.42074	0.15043	0.01	1	-3.93902	-1.13902
220 °C 120 °C	-4	0.57879	9.77356	5.61433E-4	0.01	1	-6.53902	-1.46098
220 °C 150 °C	-2.3	0.57879	5.61979	0.01725	0.01	1	-4.83902	-0.23902
220 °C 180 °C	-0.9	0.57879	2.19905	0.45213	0.01	0	-3.43902	1.63902

Sig equals 1 indicates that the means difference is significant at the 0.01 level.
Sig equals 0 indicates that the means difference is not significant at the 0.01 level.

ANOVA analysis between samples with 5 wt% CNS sintered for 3 h at different sintering temperature

One Way ANOVA

Overall ANOVA

	DF	Sum of Squares	Mean Square	F Value	Prob>F
Model	3	11.7825	3.9275	7.93434	0.0088
Error	8	3.96	0.495		
Total	11	15.7425			

Null Hypothesis: The means of all levels are equal
Alternative Hypothesis: The means of one or more levels are different
At the 0.05 level, the population means are significantly different.

Fit Statistics

R-Square	Coeff Var	Root MSE	Data Mean
0.74845	0.06717	0.70356	10.475

Means Comparisons

Tukey Test

	MeanDiff	SEM	q Value	Prob	Alpha	Sig	LCL	UCL
150 °C 120 °C	-0.5	0.57446	1.23091	0.81989	0.01	0	-3.02	2.02
180 °C 120 °C	-2.2	0.57446	5.41603	0.02096	0.01	0	-4.72	0.32
180 °C 150 °C	-1.7	0.57446	4.18511	0.07045	0.01	0	-4.22	0.82
220 °C 120 °C	-2.2	0.57446	5.41603	0.02096	0.01	0	-4.72	0.32
220 °C 150 °C	-1.7	0.57446	4.18511	0.07045	0.01	0	-4.22	0.82
220 °C 180 °C	0	0.57446	0	1	0.01	0	-2.52	2.52

Sig equals 1 indicates that the means difference is significant at the 0.01 level.
Sig equals 0 indicates that the means difference is not significant at the 0.01 level.

ANOVA analysis between samples with 5 wt% CNS sintered for 5 h at different sintering temperature

One Way ANOVA

Overall ANOVA

	DF	Sum of Squares	Mean Square	F Value	Prob>F
Model	1	18.375	18.375	49.66216	0.00214
Error	4	1.48	0.37		
Total	5	19.855			

Null Hypothesis: The means of all levels are equal
Alternative Hypothesis: The means of one or more levels are different
At the 0.05 level, the population means are significantly different.

Fit Statistics

R-Square	Coeff Var	Root MSE	Data Mean
0.92546	0.07849	0.60828	7.75

Means Comparisons

Tukey Test

	MeanDiff	SEM	q Value	Prob	Alpha	Sig	LCL	UCL
5 h 3 h	3.5	0.49666	9.96616	0.00214	0.01	1	1.2131	5.7869

Sig equals 1 indicates that the means difference is significant at the 0.01 level.
Sig equals 0 indicates that the means difference is not significant at the 0.01 level.

ANOVA analysis between samples with 5 wt% CNS sintered at 180 °C at different sintering time

APPENDIX A.3 ANOVA analysis for nanohardness results.

One Way ANOVA

Overall ANOVA

	DF	Sum of Squares	Mean Square	F Value	Prob>F
Model	3	0.00751	0.0025	2.11063	0.17717
Error	8	0.00948	0.00119		
Total	11	0.01699			

Null Hypothesis: The means of all levels are equal
Alternative Hypothesis: The means of one or more levels are different
At the 0.05 level, the population means are not significantly different.

Fit Statistics

R-Square	Coeff Var	Root MSE	Data Mean
0.4418	0.12552	0.03443	0.2743

Means Comparisons

Tukey Test

	MeanDiff	SEM	q Value	Prob	Alpha	Sig	LCL	UCL
150 °C 120 °C	0.007	0.02811	0.35213	0.99414	0.01	0	-0.11633	0.13033
180 °C 120 °C	0.0145	0.02811	0.72942	0.95296	0.01	0	-0.10883	0.13783
180 °C 150 °C	0.0075	0.02811	0.37728	0.99283	0.01	0	-0.11583	0.13083
220 °C 120 °C	0.0637	0.02811	3.2044	0.18552	0.01	0	-0.05963	0.18703
220 °C 150 °C	0.0567	0.02811	2.85227	0.25835	0.01	0	-0.06663	0.18003
220 °C 180 °C	0.0492	0.02811	2.47499	0.36087	0.01	0	-0.07413	0.17253

Sig equals 1 indicates that the means difference is significant at the 0.01 level.
Sig equals 0 indicates that the means difference is not significant at the 0.01 level.

ANOVA analysis between samples with 5 wt% CNS sintered for 3 h at different sintering temperature

One Way ANOVA

Overall ANOVA

	DF	Sum of Squares	Mean Square	F Value	Prob>F
Model	3	0.00677	0.00226	0.73925	0.55773
Error	8	0.02443	0.00305		
Total	11	0.0312			

Null Hypothesis: The means of all levels are equal
Alternative Hypothesis: The means of one or more levels are different
At the 0.05 level, the population means are not significantly different.

Fit Statistics

R-Square	Coeff Var	Root MSE	Data Mean
0.21705	0.1942	0.05526	0.28455

Means Comparisons

Tukey Test

	MeanDiff	SEM	q Value	Prob	Alpha	Sig	LCL	UCL
150 °C 120 °C	0.025	0.04512	0.78361	0.94282	0.01	0	-0.17292	0.22292
180 °C 120 °C	0.0566	0.04512	1.7741	0.61311	0.01	0	-0.14132	0.25452
180 °C 150 °C	0.0316	0.04512	0.99049	0.89413	0.01	0	-0.16632	0.22952
220 °C 120 °C	0.0566	0.04512	1.7741	0.61311	0.01	0	-0.14132	0.25452
220 °C 150 °C	0.0316	0.04512	0.99049	0.89413	0.01	0	-0.16632	0.22952
220 °C 180 °C	0	0.04512	0	1	0.01	0	-0.19792	0.19792

Sig equals 1 indicates that the means difference is significant at the 0.01 level.
Sig equals 0 indicates that the means difference is not significant at the 0.01 level.

ANOVA analysis between samples with 5 wt% CNS sintered for 5 h at different sintering temperature

One Way ANOVA

Overall ANOVA

	DF	Sum of Squares	Mean Square	F Value	Prob>F
Model	1	1.53015E-4	1.53015E-4	0.28935	0.61917
Error	4	0.00212	5.2882E-4		
Total	5	0.00227			

Null Hypothesis: The means of all levels are equal
Alternative Hypothesis: The means of one or more levels are different
At the 0.05 level, the population means are not significantly different.

Fit Statistics

R-Square	Coeff Var	Root MSE	Data Mean
0.06746	0.07379	0.023	0.31165

Means Comparisons

Tukey Test

	MeanDiff	SEM	q Value	Prob	Alpha	Sig	LCL	UCL
5 h 3 h	-0.0101	0.01878	0.76073	0.61917	0.01	0	-0.09656	0.07636

Sig equals 1 indicates that the means difference is significant at the 0.01 level.
Sig equals 0 indicates that the means difference is not significant at the 0.01 level.

ANOVA analysis between samples with 5 wt% CNS sintered at 180 °C at different sintering time

REFERENCES

1. Goosen, M.F., Applications of Chitan and Chitosan. 1996: CRC Press.
2. S. E. Byaley, et al., A review of potentially low-cost sorbents for heavy metals. Water research, 1999. **33**(11): p. 2469-2479.
3. Velásquez, C., Algunos usos del quitosano en sistemas acuosos. Revista Iberoamericana de polímeros, 2003. **4**(2): p. 91.
4. S. M. Hudson and C. Smith, Polysaccharides: Chitin and Chitosan: Chemistry and Technology of Their Use As Structural Materials, in Biopolymers from Renewable Resources, D.L. Kaplan, Editor. 1998, Springer Berlin Heidelberg: Berlin, Heidelberg. p. 96-118.
5. Smucker, R.A., Chitin primary production. Biochemical systematics and ecology, 1991. **19**(5): p. 357-369.
6. S. Arcidiacono and D.L. Kaplan, Molecular weight distribution of chitosan isolated from Mucor rouxii under different culture and processing conditions. Biotechnology and Bioengineering, 1992. **39**(3): p. 281-286.
7. Rinaudo, M., Chitin and chitosan: properties and applications. Progress in polymer science, 2006. **31**(7): p. 603-632.
8. J. G. Winterowd, J. and P.A. Sandford, Chitin and chitosan. FOOD SCIENCE AND TECHNOLOGY-NEW YORK-MARCEL DEKKER-, 1995: p. 441-441.
9. E. H. Wagener and D.W.S. Jr, Polymeric materials from renewable resources. 2010, Google Patents.
10. Kumar, M.N.R., A review of chitin and chitosan applications. Reactive and functional polymers, 2000. **46**(1): p. 1-27.
11. Kumar, C., Biofunctionalization of nanomaterials. Biofunctionalization of Nanomaterials, by Challa SSR Kumar (Editor), pp. 377. ISBN 3-527-31381-8. Wiley-VCH, November 2005., 2005. **1**.
12. O. A. Shenderova, V. V. Zhirnov, and D.W. Brenner, Carbon nanostructures. Critical Reviews in Solid State and Material Sciences, 2002. **27**(3-4): p. 227-356.
13. S. F.Wang, et al., Preparation and mechanical properties of chitosan/carbon nanotubes composites. Biomacromolecules, 2005. **6**(6): p. 3067-3072.
14. Y. Saito and S. Uemura, Field emission from carbon nanotubes and its application to electron sources. Carbon, 2000. **38**(2): p. 169-182.
15. Chung, D.D.L., Multifunctional cement-based materials. 2003: CRC Press.
16. Chung, D.D.L., Composite materials: science and applications. 2010: Springer Science & Business Media.
17. Hull, D., Materiales compuestos. 1987: Reverté.
18. Y. Hu, et al., Carbon nanostructures for advanced composites. Reports on Progress in Physics, 2006. **69**(6): p. 1847.
19. Kumar, C.S.S.R., Nanomaterials for medical diagnosis and therapy. Vol. 10. 2007: John Wiley & Sons.
20. F. Croisier and C. Jérôme, Chitosan-based biomaterials for tissue engineering. European Polymer Journal, 2013. **49**(4): p. 780-792.
21. M. Rodríguez-Vázquez, et al., Chitosan and its potential use as a scaffold for tissue engineering in regenerative medicine. BioMed research international, 2015. **2015**.

22. Vaquero, B.C., Síntesis y caracterización de los sistemas Eu2O3 y Gd2O3 por molienda mecánica, in Departamento de Ciencia e Ingeniería de los Materiales. 2011, Universidad Carlos III de Madrid p. 88.
23. K. Schönert and S. Bernotat, Size reduction. Ullmann's Encyclopedia of Industrial Chemistry, VCH Verlagsgesellschaft, Weinheim, 1998.
24. Upadhyaya, G.S., Powder metallurgy technology. 1997: Cambridge Int Science Publishing.
25. Schmid, S.R., Manufactura, ingeniería y tecnología. 2002: Pearson Educación.
26. S. F. Wang, et al., Preparation and mechanical properties of chitosan/carbon nanotubes composites. Biomacromolecules, 2005. **6**(6): p. 3067-3072.
27. A. Aryaei, A. H. Jayatissa, and A.C. Jayasuriya, Nano and micro mechanical properties of uncross-linked and cross-linked chitosan films. Journal of the mechanical behavior of biomedical materials, 2012. **5**(1): p. 82-89.
28. K. Nawrotek, et al., Tubular electrodeposition of chitosan–carbon nanotube implants enriched with calcium ions. Journal of the mechanical behavior of biomedical materials, 2016. **60**: p. 256-266.
29. M. Fardioui, et al., Bionanocomposite Materials Based on Chitosan Reinforced with Nanocrystalline Cellulose and Organo-Modified Montmorillonite, in Nanoclay Reinforced Polymer Composites. 2016, Springer. p. 167-194.
30. Cubberly, W.H., Tool and Manufacturing Engineers Handbook Desk Edition. 1989: Society of Manufacturing Engineers.
31. D. M. Escobar, A. M. Castro Ramírez, and N.A.V. Castrillón, Determining the Relation between the Proportion of the Amino Group and the Degree of Deacetylation of Chitosan. Revista de Ciencias, 2014. **18**(1): p. 73-88.
32. R. M. Hussain, M. Iman, and T.K. Maji, Determination of degree of deacetylation of chitosan and their effect on the release behavior of essential oil from chitosan and chitosan-gelatin complex microcapsules. International Journal of Advanced Engineering Applications, 2013. **6**(4): p. 4-12.
33. Broussignac, P., Chitosan: A natural polymer not well know by the industry. Chitin Ind Genie Chim, 1968. **9**: p. 1241-1247.
34. Huggins, M.L., The viscosity of dilute solutions of long-chain molecules. IV. Dependence on concentration. Journal of the American Chemical Society, 1942. **64**(11): p. 2716-2718.
35. W. Wang, et al., Determination of the Mark-Houwink equation for chitosans with different degrees of deacetylation. International Journal of Biological Macromolecules, 1991. **13**(5): p. 281-285.
36. M. R. Derrick, et al., Archive.is.
37. J. Brugnerotto, et al., An infrared investigation in relation with chitin and chitosan characterization. Polymer, 2001. **42**(8): p. 3569-3580.
38. B. Focher, et al., Alkaline N-deacetylation of chitin enhanced by flash treatments. Reaction kinetics and structure modifications. Carbohydrate Polymers, 1990. **12**(4): p. 405-418.
39. Mechatronics, S., Sartorius YDK01, YDK01-0D, YDK01B, YDK01LP, YDK01MS, YDK02MS, in Users manual.
40. I. O. Armendariz, et al., PREPARATION AND CHARACTERIZATION OF CHITOSAN/CARBON NANOTUBES COMPOSITES. Revista Mexicana de Ingeniería Química, 2009. **8**(2): p. 205-211.
41. Mogk, D. 2015; Available from: http://serc.carleton.edu/research_education/geochemsheets/techniques/SEM.html.
42. V. Cardona Trujillo and B.C.P. Quintero, Preparación y caracterización fisicoquímica y estructural de un gel conductor a base de quitosano [recurso electrónico]. 2013.

43. N. Nwe, T. Furuike, and H. Tamura, Chitin and chitosan from terrestrial organisms. Chitin, chitosan, oligosaccharides and their derivatives: Biological activities and applications, 2010: p. 3-10.
44. M. Ziegler-Borowska, et al., Effect of side substituents on thermal stability of the modified chitosan and its nanocomposites with magnetite. Journal of Thermal Analysis and Calorimetry, 2016. **124**(3): p. 1267-1280.
45. I. Mochida, et al., The Characterization and Utilization of Fullerene Soot.
46. D. de Britto and S.P. Campana-Filho, Kinetics of the thermal degradation of chitosan. Thermochimica acta, 2007. **465**(1): p. 73-82.
47. W. Feng, Y. Li, and P. Ji, Interaction of water soluble chitosan with multiwalled carbon nanotubes. AIChE Journal, 2012. **58**(1): p. 285-291.
48. Okonkwo, A.O., Development of Cost Effective Nanostructural Reinforcements for Advanced Composites. 2014.
49. H. S. Mansur, et al., Functionalized-chitosan/quantum dot nano-hybrids for nanomedicine applications: towards biolabeling and biosorbing phosphate metabolites. Journal of Materials Chemistry B, 2013. **1**(12): p. 1696-1711.
50. Scientific, H. What analysis spot size is used for a Raman microscope? 2017 [cited 2017; Available from: http://www.horiba.com/scientific/products/raman-spectroscopy/raman-academy/raman-faqs/what-analysis-spot-or-laser-spot-size-is-used-for-a-raman-microscope/.
51. M. K. Jang, et al., Physicochemical characterization of α-chitin, β-chitin, and γ-chitin separated from natural resources. Journal of Polymer Science Part A: Polymer Chemistry, 2004. **42**(14): p. 3423-3432.
52. E. C. Leonel, et al., Effect of high-energy ball milling in the structural and textural properties of kaolinite. Cerâmica, 2014. **60**(354): p. 267-272.
53. Z. Cai, et al., The effect of chitosan content on the crystallinity, thermal stability, and mechanical properties of bacterial cellulose—chitosan composites. Proceedings of the Institution of Mechanical Engineers, Part C: Journal of Mechanical Engineering Science, 2009. **223**(10): p. 2225-2230.
54. Chemical book. 2016 [cited 2017; Available from: http://www.chemicalbook.com.
55. Chávez, J.A.I., Molienda de óxidos suaves. 2008.
56. H. A. Calderon, et al., HRTEM low dose: the unfold of the morphed graphene, from amorphous carbon to morphed graphenes. Advanced Structural and Chemical Imaging, 2017. **2**(1): p. 10.
57. J.Retuert, et al., Thermal Effect On The Microhardness Of Chitosan Films. Boletín de la Sociedad Chilena de Química, 2000. **45**(2): p. 323-327.
58. C. Lee, et al., Measurement of the elastic properties and intrinsic strength of monolayer graphene. science, 2008. **321**(5887): p. 385-388.
59. L. Tsetseris, L. and S.T. Pantelides, Adatom complexes and self-healing mechanisms on graphene and single-wall carbon nanotubes. Carbon, 2009. **47**(3): p. 901-908.
60. Y. Xu, et al., Three-dimensional self-assembly of graphene oxide and DNA into multifunctional hydrogels. ACS nano, 2010. **4**(12): p. 7358-7362.
61. T. Nishino, R. Matsui, and K. Nakamae, Elastic modulus of the crystalline regions of chitin and chitosan. Journal of Polymer Science Part B: Polymer Physics, 1999. **37**(11): p. 1191-1196.
62. C. X. Wang, X. Zhou, and M. Wang, Influence of sintering temperatures on hardness and Young's modulus of tricalcium phosphate bioceramic by nanoindentation technique. Materials Characterization, 2004. **52**(4): p. 301-307.

63. I. Arzate Vazquez, et al., Mechanical characterization of edible films by nanoindentation technique. 2012.